Biochemistry, 2009, 48(46), 10905-17

Design of non-toxic analogs of cathelicidin-derived bovine anti-microbial peptide BMAP–27: The role of leucine as well as phenylalanine zipper sequences in determining its toxicity

Aqeel Ahmad[1] Sarfuddin Azmi[1$], Raghvendra M. Srivastava[1$], Saurabh Srivastava[1], Brijesh K. Pandey[1], Rubha Saxena[1], Virendra Kumar Bajpai[2] and Jimut Kanti Ghosh[1*]

[1]Molecular and Structural Biology Division
[2]Electron Microscopy Unit
Central Drug Research Institute, CSIR
Lucknow–226001, India

Running Title: The role of leucine and phenyl zipper sequences in cathelicidin-derived antimicrobial peptides

This is CDRI communication no. 7703

[*]To whom correspondence should be addressed
Tel: 091-522-2612411-18 (Ext.-4282);
Fax: 091-522-2623405;
E-mail: jighosh@yahoo.com
[$]These authors equally contributed in this work

The work was supported by the CSIR network project NWP 0005. A.A., S.A., B.K.P. acknowledge the receipt of a senior research fellowship and S.S. a junior research fellowship from CSIR, India.

Biochemistry, 2009, 48(46), 10905-17

List of Abbreviations:
hRBCs, human red blood cells; Fmoc, *N*-(9-fluorenyl) methoxycarbonyl; Chol, cholesterol; HPLC, high performance liquid chromatography; CFU, colony forming unit; PC, egg phosphatidylcholine; PG, egg phosphatidylglycerol; NBD, 4-fluoro-7-nitrobenz-2-oxa-1,3-diazole; MALDI-TOF, matrix-assisted laser desorption ionization time-of-flight; PBS, phosphate-buffered saline; MICs, minimum inhibitory concentrations; MTT, 3-(4,5-Dimethylthiazol-2-yl)-2,5-diphenyltetrazolium bromide; FRET, fluorescence resonance energy transfer; ANS, 1-anilino-8-naphthalene sulfonate.

ABSTRACT:

BMAP-27 is a cathelicidin-derived bovine anti-microbial peptide, which shows moderate cytotoxicity and potent antibacterial activity against a wide variety of microorganisms. Despite a number of studies, very little is known about the amino acid sequences of this peptide that controls its antibacterial and cytotoxic activities. A small stretches of phenylalanine and leucine zipper sequences were identified at the N- and C-terminals of the molecule respectively. In order to understand the structural and functional roles of these sequence elements several analogs of BMAP-27 were synthesized and characterized after substituting leucine/phenylalanine residue(s) at 'a' and/or 'd' positions of the leucine and phenylalanine zipper sequences respectively by alanine. The BMAP-27 analogs exhibited significantly reduced cytotoxicity against the human red blood (hRBC) and murine 3T3 cells as compared to that of the wild type peptide. Interestingly, BMAP-27 and its analogs exhibited comparable antibacterial activity against the selected Gram (+)ve and (-)ve bacteria. Moreover, BMAP-27 and its analogs showed similar localization, assembly onto the selected bacteria and induced comparable permeability in these cells. However, only BMAP-27 but not its analogs assembled and bound strongly onto the hRBCs and permeabilized them. The results indicated that not only a leucine zipper but also a phenylalanine zipper sequence plays an important role in maintaining the assembly of BMAP-27 onto the mammalian cells examined here and cytotoxic activity against them. To our knowledge this is the first report on the evaluation of structural and functional roles of a phenylalanine zipper sequence in a naturally occurring antimicrobial peptide.

Cationic antimicrobial peptides are an integral part of host immune system, which constitutes cathelicidins, defensins and other family of peptides (*1-8*). The term cathelicidin was introduced to encompass bipartite molecules containing a cathelin domain and a C-terminal antimicrobial peptide domain (*2, 4-6, 8*). Cathelin was first isolated as a 96 residue porcine peptide. The cathelicidin family shares considerable amino acid sequence homology with the cathepsin family of cysteine protease inhibitors

Cathelicidin derived peptides have a diverse range of activity against Gram-negative and Gram-positive bacteria, parasites and enveloped viruses (*9-13*). Besides activities against different microorganisms these peptides also exhibit other important biological activities that include wound healing, inhibition of tissue injury, angiogenesis, repair of skin disorder, etc (*14-17*).

To date cathelicidin derived antimicrobial peptides have been described in wide variety of vertebrates including humans (*18-20*) cattle, fish, birds etc (*4, 13, 21*). Recent studies on human cathelicidin-derived antimicrobial peptide LL-37 and its primate orthologues revealed interesting data (*22, 23*). Macaque and leaf-eating monkey RL-37 peptides contain more positive charges like other helical antimicrobial peptides found in insect, frog, and were monomeric and unstructured in bulk solution and had a potent, salt and medium independent antimicrobial activity *in vitro (22)*. In contrast, Human LL-37 is less cationic and showed a salt-dependent structuring and aggregation that influenced its antimicrobial activity and mode of action (*22, 23*). The structurally diverse cathelicidin derived antimicrobial peptides of animals provide interesting and potential models for pharmaceutical development. Several properties of the cathelicidin-derived peptides make them attractive candidates for research and drug development (*24*). They are effective killer of many microorganisms. More advantageous is their retaining bactericidal activity even at physiological or elevated salt concentration. Their synthesis is economically viable owing to the absence of disulphide bridges. Moreover their speedy rate of killing is an added merit in topical usage.

BMAP-27, an antimicrobial peptide of bovine origin also exhibits a potent and broad-spectrum anti-bacterial activity and is also cytotoxic to human erythrocytes and neutrophils (*25*). The cytotoxic property of these peptides is an indication of their poor discrimination power between the prokaryotic and eukaryotic membranes. Effort has been made to increase the selectivity of these molecules toward the microbes. BMAP-27 (1-18) was virtually devoid of cytotoxic activities and displayed antimicrobial potency slightly lower than the parent molecule (*25*). The structure-function correlation studies implied that the hydrophobic C-terminal tail is the major determinant of the cytotoxicity of BMAP molecule toward mammalian cells (*25*).

Recently, we identified and characterized an amphipathic leucine zipper motif in melittin (*26*). Substitution of heptadic leucine(s) by single or double alanine residue(s) appreciably reduced the cytotoxic activity of melittin without significantly affecting its antibacterial activity. Moreover, novel antibacterial peptides were designed on the basis of classical amphipathic leucine zipper sequence with or without alanine substitution at ‘a’ and/or ‘d’ position of the heptad repeat, which showed remarkable variation in hemolytic activity against human red blood cells but exhibited almost similar antibacterial activity (*27*). However, still it is not clear whether the leucine zipper or the heptad repeat sequences possess any role in controlling the cytotoxicity in other naturally occurring antimicrobial peptides. Toward this end, a long heptad repeat sequence was

identified in bovine antimicrobial peptide BMAP-27. The C-terminal of the sequence contains a small leucine zipper sequence and the N-terminal, a phenylalanine zipper sequence. Several alanine-substituted analogs of BMAP-27 were designed in order to investigate the role of these phenylalanine and leucine zipper sequences.

The mechanism of killing of prokaryotic and eukaryotic cells by BMAP-27 is not clear although it is believed that the peptide-induced membrane permeabilization of target cell could be the key step behind it. In order to understand the mode of action of BMAP-27 and its novel analogs peptide-induced depolarization and integrity of bacterial and mammalian cell membrane was directly measured. Also the localization and assembly of BMAP-27 and its analogs onto bacterial and human red blood cells were studied to understand the basis of their cytotoxic and antibacterial activities against the mammalian cells and bacteria.

MATERIALS AND METHODS:

Materials: Rink amide MBHA resin (loading capacity, 0.63 mmol/g) and all the N-α Fmoc and side-chain protected amino acids were purchased from Novabiochem, Switzerland. Coupling reagents for peptide synthesis like 1-hydroxybenzotriazole (HOBT), N, N′-di-isopropylcarbodiimide (DIC), 1,1,3,3-tetramethyluronium tetrafluoroborate (TBTU) and N, N′-diisopropylethylamine (DIPEA) were purchased from Sigma, India while Dichloromethane, N, N′ dimethylformamide (DMF) and piperidine were of standard grades and procured from reputed local companies. Acetonitrile (HPLC grade) was procured from Merck, India whereas trifluoroacetic acid (TFA) was purchased from Sigma, India. Egg phosphatidylcholine (PC), egg phosphatidylglycerol (PG) were procured from Northern Lipids Inc., Burnaby, British Columbia, Canada while cholesterol (Chol) was purchased from Sigma. 3,3′-Dipropylthiadicarbocyanine iodide (diS-C_3-5) and NBD (4-fluoro-7-nitrobenz-2-oxa-1, 3-diazole) -fluoride were purchased from Invitrogen (Molecular probes) (Eugene, OR). Rests of the reagents were of analytical grade and procured locally; buffers were prepared in milli Q (USF^{ELGA}) water.

Peptide Synthesis, Fluorescent labeling and Purification: Stepwise solid phase syntheses of all the peptides were carried out manually on rink amide MBHA resin (0.15 mmole) utilizing the standard Fmoc chemistry, reported earlier (*28, 29*). Labeling at the N-terminus of peptides with a fluorescent probe, cleavage of the labeled and unlabeled peptides from the resin, their precipitation and purification by reverse phase HPLC were achieved by standard procedures (*26, 29*). The purified peptides were ~95% homogeneous. Experimental molecular mass of the peptides, detected by MALDI-TOF or ESI-MS analysis, corresponded very close to the desired values.

*Assay of antibacterial activity of the peptides***:** The antibacterial activity of the peptides was assayed in sterile 96 well plate in 100μl final volume under aerobic conditions (*26, 30, 31*). In brief, 50 μL bacterial culture, grown in LB medium with 10^6 CFU/ml were added to 50μL of water containing two fold serially diluted different peptides in each well and incubated for 18-20 h at 37^0C. The peptides' antibacterial activities, expressed as their MICs (the peptide concentration which results 100% inhibition of microbial growth), were assessed by measuring the absorbance at 492 nm. The microorganisms used were Gram-positive bacteria, *Bacillus subtilis* ATCC 6633 and *Staphylococcus aureus* ATCC 9144 and Gram-negative bacterium, *Escherichia coli* ATCC 10536 and DH5α.

Bactericidal activity of BMAP-27 and its analogs were tested against *Escherichia coli* ATCC 10536 and *Bacillus subtilis* ATCC 6633 in the presence of heat inactivated serum as described by others (*32*) except FBS was used instead of human serum. The final concentration of serum in the antibacterial activity assay media was 25% v/v.

Hemolytic activity assay: Hemolytic activity of these designed peptides was assayed against fresh hRBCs that were collected in the presence of an anti-coagulant from a healthy volunteer and washed 3-4 times by PBS by a standard procedure (*26, 27, 30*). Peptides, dissolved in water, were added to the suspension of red blood cells (6% final in v/v) in PBS to the final volume of 200 μL and incubated at 37 ^{0}C for 30 min. The samples were then centrifuged for 10 min at 2000 r.p.m. and the release of hemoglobin was monitored by measuring the absorbance (A_{sample}) of the supernatant at 540 nm. For negative and positive controls, hRBCs in PBS (A_{blank}) and in 0.2% (final concentration v/v) Triton X-100 (A_{triton}) were used respectively. The percentage of hemolysis was calculated according to the following equation (*26, 30*).

Percentage of hemolysis = $[(A_{sample}-A_{blank})/(A_{triton}-A_{blank})] \times 100$

MTT assay: MTT [3-(4,5-dimethylthiazol-2-yl)-2,5-diphenyl tetrazolium bromide] assay was performed to check the toxic activity of peptides against murine 3T3 cells by a standard procedure as reported earlier (*33*). 10000 cells per well were seeded in 96 well plates and overnight incubation was done in CO2 incubator for adherence. The complete media were discarded from the plate and incomplete media were added. After that, different concentration of peptides were added and incubated for 2 hrs. Then 10 μl of MTT (conc. 5mg/ml) solutions were added in each well and again incubated for 2 hrs. Incomplete media were discarded from 96 well plates and 200 μl of DMSO were added in each well to dissolve the crystal. The well in which no peptide was added was considered as control. Reading of these samples was recorded at 550 nm by a microplate reader.

*Analysis of peptide-induced membrane damage of 3T3 and E. coli cells by flow cytometry***:** Peptide-induced membrane damage of 3T3 cells was determined by staining the cells with propidium iodide after the treatment with the peptides at 37^{0}C for 15 min. These cells were then analyzed by flow cytometry in the form of dots plot with respect to the control cells, not treated with any peptide. In order to check the membrane integrity of bacteria after peptide treatment, the cells (*E. coli* DH5α or *E. Coli* ATCC 10536**)** at mid-log phase were incubated with BMAP-27 and its alanine substituted analogs for 30 min at 37°C with constant shaking. The cells were collected by centrifugation, washed two times with PBS, and incubated further with propidium iodide at 4°C for 30 min, followed by removal of the unbound probe through washing with an excess of PBS and re-suspended in buffer. Peptide-induced damage of bacterial cells was then analyzed by flow cytometry.

*Assay of peptide-induced depolarization of hRBC and E. coli cell membrane***:** Peptide-induced depolarization of hRBCs and *E. coli* DH5α (mentioned as *E. coli* throughout the text unless stated otherwise) membrane was detected by its efficacy to dissipate the potential across these cell membranes (*34, 35*). Fresh human red blood cells (hRBCs) were collected in the presence of an anti-coagulant from a healthy volunteer and washed three times in PBS and re-suspended in the same buffer with a final cell density of ~ 3.0x 10^7 cells/ml. Human red blood cells were incubated with diS-C_3-5 probe for 1hr. When the fluorescence level (excitation and emission wavelengths set at 620 and 670 nm

respectively) of the hRBCs became stable, different amounts of each of the peptides were added to these suspensions and incubated at 37^0C for 30 min. After that peptide-induced membrane depolarization of human red blood cells were recorded. While the bacteria were grown at 37°C until it reached to its midlog phase and centrifuged followed by washing with buffer (20 mM glucose, 5 mM HEPES pH 7.3). Then bacteria were resuspended (final ~$2x10^5$ CFU/ml) in the similar buffer containing 0.1M KCL) and incubated with diS-C_3-5 probe for 1hr. When the fluorescence level of bacterial suspension became stable, different amounts of each of the peptides were added to these suspensions in order to record the peptide-induced membrane depolarization of bacterial membrane. Membrane depolarization as measured by the fluorescence recovery (F_t) was defined by the equation (*29, 36, 37*), $F_t = [(I_t - I_0)/(I_f - I_0)] \times 100$ %. Where I_f, the total fluorescence, was the fluorescence levels of cell suspensions just after addition of diS-C_3-5; I_t, observed fluorescence after the addition of a peptide at a particular concentration either to hRBCs or to *E. coli* suspensions, which were already incubated with diS-C_3-5 probe for 1hr and I_0, is the steady fluorescence level of the cell suspensions after one hr incubation with the probe. Fluorescence was monitored at 670 nm with respect to time (sec) with excitation wavelength of 620 nm. Excitation and emission slits were set at 8 and 6 nm respectively.

*Assay of peptide-induced depolarization of zwitterionic and negatively charged lipid vesicles***:** The ability of the peptides to destabilize the phospholipid bilayer was detected by their efficacy to dissipate the diffusion potential across the membrane. For this purpose both zwitterionic PC/Chol (8:1, w/w) and negatively charged PC/PG (1:1 w/w) (*38-40*) lipid vesicles were prepared in K^+ buffer (50 mM K_2SO_4/25 mM HEPES-sulfate, pH 6.8). Required amounts of the lipid vesicles were mixed with isotonic (K^+-free) Na^+-buffer (50 mM Na_2SO_4/25 mM HEPES-sulfate, pH 6.8) followed by the addition of the potential sensitive dye diS-C_3-5. Addition of valinomycin created a negative potential inside the lipid vesicles by the selective efflux of K^+ ions from the lipid vesicles. As a result of that a quenching of the fluorescence of the dye occurred. When the dye exhibited a steady fluorescence level in the presence of lipid vesicles, peptides were added. Membrane-permeability of the peptide was detected by the increase in fluorescence, which resulted from the dissipation of diffusion potential. The peptide-induced dissipation of diffusion potential was measured in terms of percentage of fluorescence recovery (F_t) by the same equation as shown in the previous section of assay of peptide-induced depolarization of hRBC and bacteria. Here I_t=the observed fluorescence after the addition of a peptide at time t (~5 min after the addition of the peptide), I_0 = the fluorescence after the addition valinomycin and I_f = the total fluorescence observed before the addition of valinomycin. Excitation and emission wavelengths of diS-C_3-5 and excitation and emission slits were the same as above.

Detection of calcein release from the calcein-entrapped lipid vesicles:

Peptide-induced calcein release from calcein-entrapped lipid vesicles has been often employed to detect the pore-forming activity of proteins and peptides. Calcein-entrapped lipid vesicles were prepared with a self-quenching concentration (60 mM) of the dye in 10 mM HEPES at pH 7.4 as reported earlier (*29, 41*). Briefly, thin film of lipid (PC/PG or PC/Chol) was re-suspended in calcein solution, vortexed for 1-2 min and then sonicated in a bath-type sonicator. The non-encapsulated calcein was removed from the liposome suspension by gel filtration using a sephadex G-50 column. Usually lipid

vesicles get diluted to approximately 10 fold after passing through a G-50 column. The eluted calcein-entrapped vesicles were further diluted in the same buffer to a final lipid concentration of ~3.0 μM for the experiment. Peptide-induced release of calcein from the lipid vesicles was detected by increase in fluorescence due to the dilution of the dye from its self-quenched concentration. Fluorescence was monitored at room temperature with excitation and emission wavelengths fixed at 490 and 520 nm respectively. Calcein release as measured by the fluorescence recovery is defined by the same equation as used to determine the peptide-induced depolarization of hRBC and bacteria or the dissipation of diffusion potential in lipid vesicles in the previous sections. However, in this case I_f, the total fluorescence, was determined after the addition of triton X-100 (0.1% final concentration) to the dye-entrapped vesicle suspension. Excitation and emission slits were fixed 8 and 6 nm respectively.

Circular dichroism experiments: CD spectra of the peptides were recorded in PBS, and in the presence of 40% TFE (in water v/v) and 1% SDS (in water w/v) by utilizing a Jasco J-810 spectropolarimeter. The samples were scanned at room temperature (~30^0 C) in a capped quartz cuvette of 0.20 cm path length in the wavelength range of 250-195 nm. The fractional helicities were calculated with the help of mean residue ellipticity values at 222 nm by the following equation (*42, 43*)**.**

.

$$F_h = \frac{[\theta]_{222} - [\theta]^0_{222}}{[\theta]^{100}_{222} - [\theta]^0_{222}}$$

Where $[\theta]_{222}$ was the experimentally observed mean residue ellipticity at 222 nm. The values for $[\theta]^{100}_{222}$ and $[\theta]^0_{222}$ that correspond to 100 and 0% helix contents were considered to have mean residue ellipticity values of –32,000 and –2,000 respectively at 222 nm.

Detection of binding of ANS to peptides:

ANS (~ 20 μM) fluorescence was recorded in the presence of each of the peptides at ~ 47.0 μM concentration. The excitation wavelength and emission wavelength range for ANS were set at 365 nm and 410-600 nm (*44*). The excitation and emission slits were fixed at 6 and 4 nm respectively.

Confocal microscopic Experiments. Localization and binding of the peptides onto the hRBCs and *E. coli* DH5α was determined with the help of their Rho-labeled analogs by employing a Zeiss LSM-510 META confocal microscope using 63x1.4 NA (oil) Plan apochromate lens. Fresh hRBCs (6% in PBS) as used in peptides' hemolytic activity assays were incubated with the same concentration of either Rho-labeled BMAP-27 or Rho- Mu-1 BMAP-27 and Rho- Mu-4 BMAP-27 for 15 min at 37^0C. Cells were washed and fixed with 2% paraformaldehyde (10 min.) after extensive washing with PBS and then confocal microscopic images of cells were taken with argon ion laser set for Rho-excitation at 561 nm. Setting of the photomultiplier was constant during the whole experiments.

Localization and binding of the peptides onto the bacterial cells was also examined with the help of Rho-labeled peptides by employing a confocal microscope. *E. coli* (~10^6 CFU/ml) in LB medium were incubated in the absence and presence of Rho labeled BMAP-27 and its analogs at their MICs for half an hour and then centrifuged, washed and analysed by the confocal microscope as described above.

*Fluorescence energy transfer experiments onto the live cells***.** FRET experiments were performed by utilizing the NBD- and Rho-labeled peptides onto the live hRBCs and *E.*

coli and analyzed by flow cytometry as reported (*45*) with the excitation and emission wavelengths set at 488 and 533 nm respectively for NBD. Equimolar amounts of NBD-labeled/unlabeled peptide (donor) and Rho-labeled peptide (acceptor) were added to the hRBCs (~3x 10^7 cells/ml) and *E. coli* (~5x10^5CFU/ml) and incubated at 37°C for 30 and 10 min. respectively. In FRET experiments fluorescence of a particular kind of cells in the presence of NBD-labeled peptide (donor) and unlabeled peptide (U) was compared to the fluorescence of the cells that was recorded in the presence of NBD-labeled peptide and the corresponding Rho-labeled peptide (acceptor).

The percentage of energy transfer exhibited by a peptide onto a particular cell was calculated by the following equation.

$$E = \{(F_{D+U} - F_{D+A})/F_{D+U}\} \times 100$$

Where E is the percentage of energy transfer, F_{D+U} is the fluorescence of the cells in the presence of NBD-labeled peptide (D) and the unlabeled peptide (U) and F_{D+A} fluorescence of the cells in the presence of NBD-labeled peptide and the corresponding Rho-labeled peptide (A).

Confocal microscopic experiments to detect the self-assembly of peptides onto bacteria and hRBCs:

To analyze the molecular proximity (aggregation) of NBD and Rho labeled peptides onto live RBCs and *E.coli,* by confocal microscopy (*46-49*) these cells were plated on poly-L-Lysine coated glass surface for adherence. In order to include more number of bacteria in the experiment of self-assembly of these peptides, *E. coli* ATCC 10536 was employed in this experiment. Equimolar amounts of NBD-labeled/unlabeled peptide (donor) and Rho-labeled peptide (acceptor) were added to the hRBCs (~3x 10^7 cells/ml) and *E. coli* (~5x10^5CFU/ml) and incubated at 37°C for 30 and 10 min. respectively and washed vigorously with PBS. Confocal microscopic images were scanned by using a Zeiss LSM-510 META confocal microscope using 63x1.4 NA (oil) Plan apochromate lens. Images were scanned by adjusting offset and voltage gain of NBD (excitation ;488nm) and Rhodamine (excitation,561nm) fluorescence. The appropriate bandpass was selected to record images. Pre-bleach NBD and Rho images were collected simultaneously following excitation at 488 nm for NBD (10.1% for *E.coli* and 9.1% for RBCs laser intensity) and at excitaion 561 nm for Rho (8.1% for *E.coli*% and 7.1% for RBCs laser intensity). The selected regions of interest were irradiated with the 561-nm laser line (100% intensity, 100 iterations, using a 488-nm/561-nm dual dichroic mirror) to photobleach rhodamine. Post-bleach NBD and rhodamine images were collected simultaneously immediately following photobleaching in line mode. FRET was measured as an increase in NBD fluorescence intensity following rhodamine photobleaching. Acceptor photobleaching method was used to assess FRET in NBD and Rhodamine labeled peptides. Co-localization of NBD and Rhodamine led to yellow images in the merged images and served as the plausible site to select the ROI (region of interest) for acceptor photobleaching. Scattered and random sites in a field were chosen as ROIs for each scan. Imgaes before acceptor photobleaching was recorded as pre-bleaching control experiment. 100% laser power was endowed for the efficient acceptor photobleaching. Two scan images after photobleaching was set to record by the software. FRET efficiency was considered positive when Fluorescence intensity of Donor $_{postbleaching}$ > Fluorescence intensity of Donor $_{prebleaching}$. Following formula was utilised to calculate FRET efficiency. FRET efficiency= (Fluorescence intensity of Donor

$_{postbleaching}$ - Fluorescence intensity of Donor $_{prebleaching}$) / Fluorescence intensity of Donor $_{postbleaching}$) × 100.

RESULTS

Design of BMAP-27 analogs

Phenylalanine zipper sequence has been recently reported in a protein (*50*), which possesses phenylalanine residue in place of leucine in the leucine zipper sequence. The 'a' and 'd' amino acids of leucine or phenylalanine zipper sequences play a crucial role in the assembly of proteins or peptides by participating in the intermolecular side chain interactions. Thus the substitution of amino acids at 'a' and 'd' positions provides a suitable way to introduce structural changes in the proteins/peptides having these sequences and also to look into its implications in the functional activity of the molecules. In order to assess the role of the phenylalanine or leucine zipper sequences, amino acids at 'a' and/or 'd' position of these heptads were substituted by alanine (Table-1). Alanine was chosen since it is known to abrogate the assembly/oligomeric properties of a protein when it is placed instead of a leucine/isoleucine at the 'a' and/or 'd' position of the heptads. Moreover, since it is a hydrophobic amino acid, amphipathic properties of the original peptide is maintained to a large extent. Among the designed analogs, the first two possess single phenylalanine or leucine residue substituted by alanine whilst in the other two analogs, two phenylalanine/leucine residues in 'a' and 'a' or 'd' positions were replaced by two alanine residues.

BMAP-27 and its analogs exhibited similar and appreciable antibacterial activity

In order to determine the antibacterial activity of BMAP-27 and its analogs peptides were tested for growth inhibiting activity in liquid cultures against Gram-positive and Gram-negative bacteria. Tetracycline was used as a positive control. Interestingly, the antibacterial activities of alanine-substituted analogs were close to that of BMAP-27 (Table-2). The results showed that the antibacterial activity of BMAP-27 was almost intact after the substitution of leucine/phenylalanine residue(s) by alanine residue(s) in its 'a' and/or 'd' position of leucine/phenylalanine zipper sequence. Antibacterial activities of these peptides were evaluated against one Gram positive (*B. subtilis* ATCC 6633) and one Gram-negative (*E. Coli* ATCC 10536) bacteria in the presence of serum. BMAP-27 and its analogs showed comparable bactericidal activity against these selected bacteria in the presence of serum (Supplementary Table-1). However, the MIC values of the peptides in the presence of serum against *E. Coli* ATCC 10536 were around double to that in the absence of serum while the MIC values against *B. subtilis* ATCC 6633 in the presence of serum were almost four times to that in the absence of serum. The data indicated that serum proteins inhibited the anti-bacterial activity of BMAP-27 and its analogs against these selected bacteria to varying degree. Furthermore, bactericidal activities of these Rho-labeled peptides were assayed against the selected Gram-positive and Gram-negative bacteria (Supplementary Figure-1), which suggested that Rho-labeling did not significantly affect the activity of BMAP-27 and its analogs.

Alteration of cytotoxic activity of BMAP-27 after substitution of phenylalanine/leucine by alanine at 'a' and/or 'd' position of phenylalanine/leucine zipper sequence

Cytotoxic activity of BMAP-27 and its analogs was determined by measuring their hemolytic activity against the human red blood cells and the viability of murine 3T3 cells

in their presence. BMAP-27 exhibited the maximum hemolytic activity against hRBCs (Figure 1A). However, the hemolytic activity drastically reduced in the BMAP-27 analogs in which single or double phenylalanine/leucine residue(s) was replaced by alanine residue(s). Thus the data clearly suggested that these phenylalanine or leucine residues at the 'a' and/or 'd' position of the BMAP-27 heptads play a crucial role in maintaining the hemolytic activity of the peptide.

The viability of 3T3 cells in the presence of BMAP-27 and its analogs was detected by measuring the mitochondrial dehydrogenese activity of these cells by MTT assay. 3T3 cells were least viable in presence of BMAP-27 as compared to the other peptides indicating higher cytotoxicity of the wild type peptide than its analogs. Thus the designed analogs with substitution of phenylalanine/leucine in the phenylalanine /leucine zipper sequences exhibited a similar trend in the reduction of cytotoxicity against the 3T3 cells (Figure 1B) as was observed in case of determining their hemolytic activity against the hRBCs. The results thus suggested that the substitution of phenylalanine/leucine at 'a' and/or 'd' position in the phenylalanine or leucine zipper sequence not only altered the toxic activity of BMAP-27 against the hRBCs but also against the mouse fibroblast 3T3 cells probably implicating a role of these sequences in maintaining cytotoxic activity of this antimicrobial peptide. Altogether the data indicated a possible role of both leucine and phenylalanine zipper sequences in the cytotoxic activity of BMAP-27.

Unlike BMAP-27 its analogs selectively damaged the membrane organization of bacteria but not the mammalian cells

The changes in membrane organization of murine fibroblasts 3T3 cells and bacteria, *E. coli* in the presence of BMAP-27 and its analogs was probed by incubating the peptide-treated cells with the DNA intercalating dye propidium iodide (PI). PI is impermeable to normal viable cells and it can enter only into those cells and interact with their DNA whose membranes are damaged. PI staining of 3T3 cells following the treatment of the peptides showed that BMAP-27 damaged the membrane organization of these cells to the highest extent, while its analogs were appreciably less active (Figure 2).

However, interesting results were obtained when *E. coli* cells were stained with PI following the treatment of BMAP-27 and its alanine substituted analogs. Unlike in case of PI staining of 3T3 cells after the treatment of the peptides, *E. coli* cells treated with either BMAP-27 (3.5 μM) or its analogs showed an almost similar shift (~80%) of the dots to the upper right side (Figure 3) indicating a similar damage of membrane organization of the bacteria by each of these peptides. The data suggested that the substitution of phenylalanine and leucine by alanine in the phenylalanine and leucine zipper motifs respectively impaired the ability of BMAP-27 only to damage the membrane organization of 3T3 cells but not bacteria, *E. coli*. Furthermore, peptide-induced membrane damage of *E. Coli* ATCC 10536 was studied in the presence of the NBD-labeled BMAP-27 and its selected alanine substituted analog and compared it with the damage induced by their unlabeled versions (Supplementary Figure-1). The results indicated that no significant difference was observed between the membrane damage caused by the unlabeled peptide and the corresponding unlabeled version.

Contrasting differences between BMAP-27 and its analogs in depolarizing hRBCs while these peptides depolarized E. coli to a similar extent

Membrane depolarization of bacterium, *E. coli* and mammalian cell, hRBCs was determined in the presence of BMAP-27 and its analogs in order to understand the

possible mode of action and the molecular basis of their contrasting cytotoxic activity but very similar antibacterial activity. BMAP-27 and its analogs induced depolarization of *E. coli* and hRBCs membrane was determined with the help of a potential sensitive dye diS-C_3-5. Depolarization of each of these cell membranes in the presence of BMAP-27 and its analogs was measured with respect to fluorescence recovery induced by these peptides at different concentrations as described in Materials & Methods section. BMAP-27 and its analogs induced very similar membrane depolarization in *E. coli* (Figure 4A) as indicated by the similar fluorescence recovery induced by these peptides. However, onto human red blood cells alanine substituted analogs of BMAP-27 induced significantly lower membrane depolarization than that of wild type BMAP-27 (Figure 4B). Thus the results indicated that although the substitution of leucine or phenylalanine by alanine had almost negligible effect toward the peptide-induced depolarization in *E. coli* it significantly impaired the BMAP-27 induced depolarization of hRBC membrane.

Differences between BMAP-27 and its analogs in permeabilizing the zwitterionic lipid vesicles but not in negatively charged lipid vesicles

Often lipid vesicles with zwitterionic (like PC/Chol) and negatively charged lipids (like PE/PG or PC/PG) are employed to mimic the eukaryotic and prokaryotic cell membrane respectively. Therefore, to understand the basis of differences and similarities in BMAP-27 and its alanine-substituted analogs induced depolarization of hRBCs, and bacteria respectively, permeabilization of both zwitterionic PC/Chol and negatively charged PC/PG in the presence of these peptides was examined by measuring the peptides induced depolarization of these lipid vesicles as depicted in the Materials and Methods. Increase in fluorescence of the probe, which resulted from the dissipation of diffusion potential across the membrane indicated the peptide-induced permeability of a particular kind of lipid vesicles. Panel A of Figure 5 shows experimental profiles of depolarization of PC/Chol vesicles by BMAP-27 and its analogs at a particular peptide concentration while the plot of fluorescence recovery, which is a measure of peptide-induced permeabilization of these lipid vesicles vs peptide concentration has been presented in Panel C Figure 5. It is evident from the fluorescence enhancement of the probe following the addition of the peptides that wild type BMAP-27 appreciably permeabilized PC/Chol vesicles. However, all the single and double alanine substituted analogs were significantly less active than the wild type molecule clearly suggesting that alanine substitution significantly impaired the ability of BMAP-27 to permeabilize the zwitterionic lipid vesicles. Interestingly, contrasting results were observed when the depolarization of negatively charged lipid vesicles was measured in the presence of these peptides. As evident from the representative fluorescence profiles at a particular peptide concentration (Panel B, Figure 5) and the plot of fluorescence recovery vs peptide concentrations (Panel D), BMAP-27 and its analogs possess significant and almost similar efficacy to permeabilize the PC/PG lipid vesicles.

In order to further characterize BMAP-27 and its analogs induced permeability of zwitterionic and negatively charged lipid vesicles, release of calcein from calcein-entrapped both kinds of lipid vesicles in the presence of these peptides were examined. BMAP-27 appreciably induced release of calcein from calcein-entrapped both zwitterionic PC/Chol and negatively charged PC/PG lipid vesicles as evidenced by the representative calcein release profiles (Supplementary Figure 2A and B) and plot of fluorescence recovery data (Supplementary Figure –2C and D). On the other hand,

alanine-substituted BMAP-27 analogs were as efficient as the wild type molecule in releasing calcein from calcein entrapped PC/PG lipid vesicles (profiles at a particular concentration, Supplementary Figure-2B**;** fluorescence recovery plot, Supplementary Figure-2D). However, similar to membrane depolarization study these analogs induced the release of calcein from zwitterionic PC/Chol vesicles to a much lesser extent than to BMAP-27 (calcein release profiles, Supplementary Figure-2A-; fluorescence recovery plot, Supplementary Figure-2C). Altogether the results of membrane-depolarization and calcein release from calcein-entrapped lipid vesicles indicated that the alanine-substituted BMAP-27 analogs induced reduced permeabilization only in zwitterionic lipid vesicles but not in the negatively charged lipid vesicles.

Induction of alpha helical structure of BMAP-27 and its analogs in the membrane mimetic environments

Circular dichroism (CD) experiments were performed to study the secondary structures of BMAP-27 and its analogs in aqueous environment (phosphate buffered saline, PBS, pH 7.4) and in the membrane mimetic environments like SDS micelles and 40% TFE (v/v in water). The peptides did not adopt significant helical structures in PBS (data not presented). However, both in 40% TFE and 1% SDS BMAP-27 and its analogs adopted appreciable helical structures as evident from the shape of the spectra (Figure 6). Considering the mean residue ellipticity values at 222 nm it appears that in 40% TFE BMAP-27 and it analogs adopted 30-45% helical structures whereas in 1% SDS the peptides showed 33-43% helicity.

Significant difference in ANS fluorescence of BMAP-27 and its analogs

ANS is a hydrophobic fluorescent probe, which is practically non-fluorescent in aqueous environment. However, in hydrophobic environment its fluorescence enhances significantly with shift of emission maximum to shorter wavelength. Self-association of BMAP-27 and its analogs in aqueous environment was probed by ANS as reported earlier (*44*). In PBS ANS showed negligible fluorescence. However, in the presence of BMAP-27, fluorescence of ANS increased significantly with emission maximum at shorter wavelength at ~485 nm, indicative of binding of the probe to the hydrophobic peptide environment probably resulted by the aggregation of the peptide (Supplementary Figure-3*)*. Interestingly, a totally distinct result was observed when ANS fluorescence was recorded in the presence of BMAP-27 analogs. Single and double alanine substituted BMAP-27 analogs induced much lesser enhancement of ANS fluorescence and lesser shift of its emission maximum (~500.5 nm) toward the shorter wavelength as compared to that observed for the parent molecule (Supplementary Figure-3). The data clearly indicated that BMAP-27 was much more self-aggregated than its alanine substituted analogs in aqueous environment. In other words, substitution of leucine and phynylalanine by alanine in the corresponding zipper sequences disturbed the self-association of BMAP-27. Interestingly, a scrambled BMAP-27 analog (SCR-BMAP-27) having the same amino acid composition as BMAP-27 with only minor alteration in the zipper sequences also induced lesser shift towards shorter wavelength (emission maximum, ~494 nm) and significantly lesser enhancement of fluorescence of ANS than that in the presence of BMAP-27, suggesting a possible role of these zipper sequences in the self-association of BMAP-27 in aqueous environment.

Contrasting localization of BMAP-27 and its analogs onto hRBC cells but not in bacteria

The effect of substitution of leucine/phenylalanine by alanine in the leucine/phenylalanine zipper sequence of BMAP-27 on its localization onto hRBCs was studied (left hand side, Figure 7) by confocal microscopic technique. Bright red fluorescence of Rho-BMAP-27 was observed onto the hRBCs indicating strong binding of BMAP-27 molecules to these cells. However, the hRBCs after incubation with Rho-Mu-1 BMAP-27 showed much weaker fluorescence and the cells after treatment with Rho-Mu-4 BMAP-27 exhibited the least fluorescence. The data clearly suggested that substitution of phenylalanine and leucine residue(s) by alanine residue(s) in the BMAP-27 heptad progressively disturbed the binding and localization of the molecule onto the human red blood cells.

Interestingly, while looking at the localization of these peptides onto the bacteria, strong red fluorescence of Rho-BMAP-27 as well as its Rho-labeled alanine-substituted analogs was observed onto the *E. coli* cells (right hand side, (Figure 7). Thus confocal microscopic studies showed a similar binding and localization of BMAP-27 and its analogs onto bacteria when treated at ~70% of the MIC concentrations. Moreover, when confocal microscopic images of *E. coli* were recorded after treatment with the Rho-labeled peptides at MIC concentrations a damage of the bacterial cell membrane with change in their morphology was observed. The data clearly indicated that these peptides targeted the bacterial membrane and further suggested that Rho-labeling did not disturb the activity of these peptides against the bacteria. Taken together confocal microscopic studies revealed that the substitution of leucine/phenylalanine by alanine in the leucine/phenylalanine zipper sequence had significant effect on the binding and localization of BMAP-27 onto the hRBC cells although it had negligible influence on the localization of the peptide onto *E. coli* cells.

Alanine substituted BMAP-27 analogs adopted weaker assembly onto hRBCs while they assembled as good as BMAP-27 onto E. coli

The role of assembly of antimicrobial peptides onto bacteria and mammalian cells in determining their antibacterial and cytotoxic activities is not well understood. Toward this end the assembly of BMAP-27 and its selected analogs onto the live hRBCs and *E. coli* was examined with the help of fluorescence resonance energy transfer experiments by employing NBD- and Rho-labeled version of the peptides as energy donors and acceptors respectively. Fluorescence of *E. coli* and hRBCs in the presence of different fluorescent-labeled peptides was measured by a flow cytometer. NBD-BMAP-27 appreciably bound to the hRBCs as indicated by the significant fluorescence levels (X-axis value) of these cells (Figure 8) when incubated with the labeled peptide. However, when Rho-labeled BMAP-27 was added to NBD-BMAP-27-bound hRBCs, appreciable energy transfer was observed as evidenced by the decrease in NBD-fluorescence of these cells (the shift of fluorescence peak toward left hand side, lower value). Thus the data suggested that BMAP-27 self-assembled onto the hRBC cells (Figure 8). In contrast, the binding of both the NBD-labeled alanine-substituted analogs, Mu-1 BMAP-27 and Mu-4 BMAP-27 was appreciably weaker than the wild type BMAP-27 as indicated by the less intense fluorescence level (the X-axis value) of the cells in their presence. Furthermore, the decrease in NBD fluorescence of the hRBCs when these unlabeled BMAP-27 analogs were replaced by their Rho-labeled version was less than that observed in case of the wild type NBD-BMAP-27 indicating a weaker energy transfer events between the donor and acceptor labeled BMAP-27 analogs as compared to that of wild type BMAP-27. Thus

the results indicated that the alanine substituted BMAP-27 analogs did not self-assemble appreciably onto live hRBC cells unlike their parent molecule. Interestingly, when the assembly of BMAP-27 and its two selected analogs was examined onto live *E. coli* in a similar way by fluorescence energy transfer experiments both BMAP-27 and its alanine substituted analogs showed appreciable and comparable self-assembly onto the bacteria (right hand side, Figure 8). This is evidenced from the observation that for all three peptides, the NBD-fluorescence of *E. coli* cells decreased appreciably following the addition of the corresponding Rho-labeled peptide in place of the respective unlabeled peptide. A quantitative analysis of these FRET experiments was performed by utilizing the mean fluorescence of the cells in the presence of NBD-labeled and the corresponding unlabeled peptide (F_{D+U}) and the mean fluorescence of the cells in the presence of NBD- and Rho-labeled peptides (F_{D+A}), described in the Materials & Methods. As shown in Figure-8G BMAP-27 showed an energy transfer of ~31% onto hRBCs whereas the selected analogs (Mu-1 BMAP-27 and Mu-4 BMAP-27) showed only 4 and 2% energy transfer onto the same cells indicating a significant difference between the wild type and mutant peptides in their self-assembly onto hRBCs. In contrast, all three peptides showed appreciable and very similar energy transfer (~55%) suggesting that all these peptides self-assembled to a similar extent onto *E. coli* unlike in case of hRBCs.

Self-assembly of BMAP-27 and its analogs was further probed by confocal microscopic studies (*46*, *47*) by looking at the enhancement of donor (NBD-labeled peptide) fluorescence as a result of photobleaching of the acceptor molecule (corresponding Rho-labeled peptide) onto *E. coli* and hRBCs (Supplementary Figure-4). A significant increase in the NBD fluorescence at the site of acceptor photobleaching was observed for both BMAP-27 and its analogs onto *E. coli(*Supplementary Figure-4A and B). The data clearly indicated energy transfer between NBD and Rho-labeled BMAP-27 as well as its analogs resulting from the self-assembly of these individual peptide molecules onto *E. coli*. However, similar energy transfer experiments onto hRBCs revealed self-association of only wild type BMAP-27 (Supplementary Figure-4C and D). BMAP-27 analogs bound very weakly to hRBCs and did not self-assemble appreciably onto hRBCs (Supplementary Figure-4C and D). Altogether confocal microscopic studies supported the trend of FRET experiments data by flow cytometry onto the live *E. coli* and hRBCs.

DISCUSSION:

The results showed the identification and characterization of a small stretch of phenylalanine and a leucine zipper sequence at the N- and C-terminal of a long heptad repeat in bovine antimicrobial peptide BMAP-27. It is evident from the data that the substitution of either phenylalanine or leucine at the 'a' and/or 'd' position of phenylalanine or leucine zipper sequences severely reduced the toxic activity of BMAP-27 without affecting its antimicrobial activity. The results clearly suggested the role of these sequences in maintaining the cytotoxic activity of cathelicidin-derived bovine antimicrobial peptides BMAP-27. A decrease in bactericidal activity of BMAP-27 and its analogs against the selected bacteria in the presence of serum (Supplementary Table-1) indicated an interference by plasma proteins toward the antimicrobial activity of the peptides as was also observed in case LL-37 (*51*). Labeled peptides retained the antibacterial activity against the bacteria and also damaged their membrane organization like their unlabeled versions suggesting that labeling of BMAP-27 and its analogs did not

disturb their functional activities (Supplementary Figure-1). In order to explore further evidence on the role of these zipper sequences on maintaining cytotoxicity of BMAP-27, a scrambled BMAP-27 analog (SCR-BMAP-27) was designed which possess the same amino acid composition as the original peptide except minor alteration in the zipper sequence (Supplementary Figure-5). The positions of polar and charged residues in this analog were the same as in the wild type peptide. Since SCR-BMAP-27 possesses the same amino acid composition as the wild type peptide and only the positions of the hydrophobic amino acids were interchanged with each other to include a minor modification in the leucine and phenylalanine zipper sequences, this analog retains the amphipathic properties of BMAP-27. Helical wheels of BMAP-27, SCR-BMAP-27 and a double alanine substituted analog (Mu-3 BMAP-27) are shown in Supplementary Figure-5. However, despite having the same amino acid composition as BMAP-27, SCR-BMAP-27 showed drastically reduced hemolytic activity against hRBCs and cytotoxicity against 3T3 cells (Supplementary Figure -5) confirming the crucial role of the leucine and phenylalanine zipper sequences in maintaining the cytotoxicity of BMAP-27. Yet SCR-BMAP-27 exhibited comparable antibacterial activity to BMAP-27 or its analogs. This peptide damaged the membrane organization of *E. coli* but not of 3T3 cells (Supplementary Figure-5).

Hydrophobicity of antimicrobial peptides is often utilized to explain the hemolytic activity of the antimicrobial peptides, which is a measure of their cytotoxicity. However, the molecular basis of reduction in toxicity of an antimicrobial peptide as a result of decrease in its hydrophobicity is not well known. The substitution of single and double leucine or phenylalanine residue(s) by single or double alanine residue(s) will not drastically reduce the hydrophobicity of the twenty seven-residue BMAP-27. However, even after single amino acid substitution a drastic reduction in hemolytic activity of BMAP-27 was observed; practically all the single or double alanine-substituted BMAP-27 analogs showed no detectable hemolytic activity (Figure 1) up to ~ 50 μM peptide concentration used for this experiment. The results clearly suggest that the decrease in hydrophobicity of BMAP-27 as a result of these amino acid substitutions cannot alone explain the severely reduced toxicity of BMAP-analogs. The hemolytic activity data of SCR-BMAP-27 confirms that just maintaining the composition or hydrophobicity or amphipathic property is not enough to preserve the cytotoxicity of BMAP-27.

The possible mechanism of action of BMAP-27 and its analogs to kill the microorganisms and mammalian cells was studied by directly looking into the ability of the peptides to depolarize these cells. BMAP-27 depolarized both hRBC and *E. coli* with significant efficacy, which also matched with its non-cell-selective both hemolytic and antibacterial activities. All the alanine-substituted analogs also induced appreciable permeability in the bacteria, which was comparable to that of the wild type BMAP-27. Interestingly, the substitution of phenylalanine or leucine at the ‘a’ and/or ‘d’ position of the phenylalanine or leucine zipper sequences drastically reduced the BMAP-27-induced depolarization of hRBCs, which probably points out toward the basis of decrease in toxic activity of BMAP-27 analogs against the hRBCs. Propidium iodide (PI) staining of 3T3 and bacterial cells after the treatment of BMAP-27 and its analogs support the peptide-induced killing and depolarization of these cells**.**

The flow cytometric studies of PI staining (Figures 2 and 3) and peptide-induced depolarization of *E. coli* and hRBCs (Figure 4) indicate that probably BMAP-27

primarily interact with the membrane of the target cells in order to exhibit cytotoxic and antibacterial activities and peptide-induced permeabilization of the target cells is the key event associated with the killing of these cells. Furthermore, the observation of damage of the cell membrane and change in morphology by confocal microscopic studies of *E. coli* at MIC of BMAP-27 (Figure 7) and its analogs supported that these peptides could target the cell membrane of bacteria to exhibit their antibacterial activity. The ability of BMAP-27 to bind and localize onto the cell membrane of both mammalian and bacterial cells probably assists in the permeabilization of both kinds of cell membrane. That substitution of leucine/phenylalanine by alanine impaired the localization of BMAP-27 onto the hRBCs, could contribute in the weak permeability of these cells in the presence of BMAP-27 analogs. The similarities of the results of the membrane permeability studies of selected mammalian cells and bacteria (Figure 4) with the corresponding mimetic lipid vesicles (Figure 5, Supplementary Figure-2) probably indicate a key role of lipid-peptide interaction in determining the activity of BMAP-27 and its analogs. Circular dichroism studies (Figure 6) indicated both BMAP-27 and its analogs adopted appreciable helical structures in membrane mimetic environments. Nevertheless differences between BMAP-27 and its analogs in their self-assembly onto hRBCs but not *E. coli* was observed (Figure 8, Supplementary Figure-4), which could significantly contribute in the distinct nature of peptide-induced permeability of the mammalian cells and bacteria. However, the exact stage of interaction of BMAP-27 or its analogs with bacterial membrane at which the peptides self-assemble onto bacteria is unclear. We cannot rule out a possibility that these peptide molecule first bind onto the surface of bacteria like carpet and then self-assemble with the neighboring molecules in course of disrupting the bacterial membrane.

Altogether, the data suggest that the substitution of leucine/phenylalanine by alanine at the leucine or phenylalanine zipper sequence of BMAP-27 impaired the localization and assembly of the peptide onto the hRBCs, which could contribute in impairing the ability of BMAP-27 to permeabilize these cells and probably therefore its analogs exhibited weak hemolytic activities. In contrast, both BMAP-27 and its analogs showed similar binding, localization and assembly onto *E. coli*, which probably resulted in their similar ability to depolarize the bacteria and thus the peptides exhibited similar lytic activity against the bacteria. Interesting differences were observed between BMAP-27 and its alanine substituted analogs in their self-assembly in aqueous PBS. ANS binding (Supplementary Figure-3) clearly demonstrated that BMAP-27 was significantly more aggregated than its analogs supporting the role of these zipper sequences in the assembly of a peptide in aqueous environment as already shown by others for proteins/peptides. Moreover, that more aggregated peptide is more toxic than the less aggregated peptide in aqueous environment showed similarity with previous studies (*26, 27, 52*)**.**

The molecular basis of assembly of alanine-substituted analogs of BMAP-27 onto bacteria is not well understood. The primary difference between the outer membrane of mammalian cell and that of bacterial membrane is that the former contains zwitterionic lipids and is electrically neutral while the latter is negatively charged due to presence of LPS/lipoteichoic acid and negatively charged lipids. We speculate that the hydrophobic interaction between the adjacent leucine and phenylalanine residues of the leucine and phenylalanine zipper sequence of BMAP-27 is very crucial for maintaining self-assembly

of the peptide onto the mammalian cell membrane. Since BMAP-27 is highly positively charged (8 positive charges at physiological pH) the peptide molecules could be attracted to the bacterial membrane. Probably, at some peptide concentration onto the bacterial membrane surface they can come close to each other and self-assemble. Probably, the electrostatic interaction between the cationic residues of the peptides and the negative charge of the bacterial membrane compensate the loss of hydrophobic interaction between the leucine residues and aromatic phenylalanine residues.

The results of reduction in hemolytic activity of BMAP-27 showed remarkable similarity with our previously reported results on the hemolytic activity of alanine-substituted analogs of melittin and LZP peptide (*26, 27*). Besides, hemolytic activity, cytotoxic activity of BMAP-27 and its analogs was checked against murine 3T3 cells by MTT assay, which also showed appreciable decrease after the substitution of phenylalanine or leucine by alanine in the phenylalanine and leucine zipper sequence of BMAP-27. Collectively, the data indicated towards a general role of these heptad repeat sequences in maintaining the toxic activity of the antimicrobial peptides containing these sequence elements. One of the salient features of the BMAP-27 sequence is the presence of a phenylalanine zipper sequence. The results presented here demonstrated that the phenylalanine zipper sequence also plays a similar role as the leucine zipper sequence in the assembly of BMAP-27 onto hRBCs. A previous study showed that 21-residue alanine, lysine and phenylalanine rich peptides containing phenylalanine zipper sequence self-assembled in aqueous environment and exhibited toxicity against 3T3 cells (*44*). A magainin variant, MSI-78 containing a phenylalanine zipper was reported to form dimer in DPC micelle by NMR study (*53*). However, permeabilization of mammalian cells and bacteria or assembly and localization of these peptides onto any of the cells are not known to our knowledge.

In summary taking into the consideration of the previous results, it appears that leucine or phenylalanine zipper sequence elements play a predominant role in maintaining the cytotoxic activity of BMAP-27 against the mammalian cells. Thus the presence of leucine/phenylalanine zipper sequence or probably a heptad repeat in general provides a convenient way of incorporating a minor amino acid substitution to design peptides with selective lytic activity against microorganisms.

ACKNOWLEDGEMENT: The authors are extremely thankful to A. L. Vishwakarma for recoding the flow cytometry profiles. Manish Singh, Electron Microscopy Unit, CDRI is acknowledged for assistance in recording the confocal microscopic images.

SUPPORTING INFORMATION AVAILABLE:

Antibacterial activity of BMAP-27 and its analogs against a Gram positive and a Gram negative bacteria was examined in the presence of serum (Supplementary Table-1). The data show a varying degree of inhibition of bactericidal activity of the peptides by the plasma proteins present in the serum. Activity of labeled peptides was determined to check whether labeling of BMAP-27 and its analogs by fluorescent probes disturbed their functional property or not. Panel A to G (Supplementary Figure-1) show that E. coli. ATCC 10536 bound to NBD-labeled peptides were also stained by PI, which was comparable to the staining of bacteria by their unlabeled versions. Panel H shows that rhodamine labeling of BMAP-27 and its analogs did not have significant effect on their bactericidal activities. Pore-forming property of BMAP-27 and its analogs was

determined by monitoring the peptides-induced release of calcein from calcein-entrapped zwitterionic (PC/Chol) and negatively charged (PC/PG) lipid vesicles (Supplementary Figure-2). ANS binding of peptides indicated that BMAP-27 was more aggregated in aqueous environment than its analogs ((Supplementary Figure-3). Self-assembly of BMAP-27 and its selected analogs onto bacteria and hRBCs was examined by confocal microscopic studies with the help of photobleaching of acceptor molecules ((Supplementary Figure-4). BMAP-27 as well as its analogs self-assembled onto bacteria. However, BMAP-27 analogs did not bind or self-assemble appreciably to hRBCs. Amino acid sequence of a BMAP-27 analogs, which possesses the same amino acid composition as the parent molecule with only minor amino acid modification in the zipper sequences has been shown in Supplementary Figure-5 along with its bactericidal, cytotoxic activities. Furthermore, the ability of this analog (SCR-BMAP-27) to induce damages in membrane organization of bacteria and mammalian cell was studied [Supplementary Figure-5 (5)]. The supporting information are accessed free of charge online at http://pubs.acs.org . These materials are available free of charge via the Internet at http://pubs.acs.org.

REFERENCES*:*

(1) Boman, H. G. (1995) Peptide antibiotics and their role in innate immunity. *Annu Rev Immunol 13*, 61-92.

(2) Ramanathan, B., Davis, E. G., Ross, C. R., and Blecha, F. (2002) Cathelicidins: microbicidal activity, mechanisms of action, and roles in innate immunity. *Microbes Infect 4*, 361-372.

(3) Lehrer, R. I., Lichtenstein, A. K., and Ganz, T. (1993) Defensins: antimicrobial and cytotoxic peptides of mammalian cells. *Annu Rev Immunol 11*, 105-128.

(4) Hancock, R. E. (2001) Cationic peptides: effectors in innate immunity and novel antimicrobials. *Lancet Infect Dis 1*, 156-164.

(5) Risso, A. (2000) Leukocyte antimicrobial peptides: multifunctional effector molecules of innate immunity. *J Leukoc Biol 68*, 785-792.

(6) Gennaro, R., and Zanetti, M. (2000) Structural features and biological activities of the cathelicidin-derived antimicrobial peptides. *Biopolymers 55*, 31-49.

(7) Gennaro, R., Skerlavaj, B., and Romeo, D. (1989) Purification, composition, and activity of two bactenecins, antibacterial peptides of bovine neutrophils. *Infect Immun 57*, 3142-3146.

(8) Bals, R., and Wilson, J. M. (2003) Cathelicidins--a family of multifunctional antimicrobial peptides. *Cell Mol Life Sci 60*, 711-720.

(9) Zanetti, M., Gennaro, R., and Romeo, D. (1995) Cathelicidins: a novel protein family with a common proregion and a variable C-terminal antimicrobial domain. *FEBS Lett 374*, 1-5.

(10) Travis, S. M., Anderson, N. N., Forsyth, W. R., Espiritu, C., Conway, B. D., Greenberg, E. P., McCray, P. B., Jr., Lehrer, R. I., Welsh, M. J., and Tack, B. F.

(2000) Bactericidal activity of mammalian cathelicidin-derived peptides. *Infect Immun 68*, 2748-2755.

(11) Lehrer, R. I., and Ganz, T. (2002) Cathelicidins: a family of endogenous antimicrobial peptides. *Curr Opin Hematol 9*, 18-22.

(12) Durr, U. H., Sudheendra, U. S., and Ramamoorthy, A. (2006) LL-37, the only human member of the cathelicidin family of antimicrobial peptides. *Biochim Biophys Acta 1758*, 1408-1425.

(13) Zasloff, M. (2002) Antimicrobial peptides of multicellular organisms. *Nature 415*, 389-395.

(14) Carretero, M., Escamez, M. J., Garcia, M., Duarte, B., Holguin, A., Retamosa, L., Jorcano, J. L., Rio, M. D., and Larcher, F. (2008) In vitro and in vivo wound healing-promoting activities of human cathelicidin LL-37. *J Invest Dermatol 128*, 223-236.

(15) Dorschner, R. A., Pestonjamasp, V. K., Tamakuwala, S., Ohtake, T., Rudisill, J., Nizet, V., Agerberth, B., Gudmundsson, G. H., and Gallo, R. L. (2001) Cutaneous injury induces the release of cathelicidin anti-microbial peptides active against group A Streptococcus. *J Invest Dermatol 117*, 91-97.

(16) Koczulla, R., von Degenfeld, G., Kupatt, C., Krotz, F., Zahler, S., Gloe, T., Issbrucker, K., Unterberger, P., Zaiou, M., Lebherz, C., Karl, A., Raake, P., Pfosser, A., Boekstegers, P., Welsch, U., Hiemstra, P. S., Vogelmeier, C., Gallo, R. L., Clauss, M., and Bals, R. (2003) An angiogenic role for the human peptide antibiotic LL-37/hCAP-18. *J Clin Invest 111*, 1665-1672.

(17) Lande, R., Gregorio, J., Facchinetti, V., Chatterjee, B., Wang, Y. H., Homey, B., Cao, W., Wang, Y. H., Su, B., Nestle, F. O., Zal, T., Mellman, I., Schroder, J. M., Liu, Y. J., and Gilliet, M. (2007) Plasmacytoid dendritic cells sense self-DNA coupled with antimicrobial peptide. *Nature 449*, 564-569.

(18) Gudmundsson, G. H., Agerberth, B., Odeberg, J., Bergman, T., Olsson, B., and Salcedo, R. (1996) The human gene FALL39 and processing of the cathelin precursor to the antibacterial peptide LL-37 in granulocytes. *Eur J Biochem 238*, 325-332.

(19) Frohm, M., Agerberth, B., Ahangari, G., Stahle-Backdahl, M., Liden, S., Wigzell, H., and Gudmundsson, G. H. (1997) The expression of the gene coding for the antibacterial peptide LL-37 is induced in human keratinocytes during inflammatory disorders. *J Biol Chem 272*, 15258-15263.

(20) Johansson, J., Gudmundsson, G. H., Rottenberg, M. E., Berndt, K. D., and Agerberth, B. (1998) Conformation-dependent antibacterial activity of the naturally occurring human peptide LL-37. *J Biol Chem 273*, 3718-3724.

(21) Hancock, R. E., and Lehrer, R. (1998) Cationic peptides: a new source of antibiotics. *Trends Biotechnol 16*, 82-88.

(22) Zelezetsky, I., Pontillo, A., Puzzi, L., Antcheva, N., Segat, L., Pacor, S., Crovella, S., and Tossi, A. (2006) Evolution of the primate cathelicidin. Correlation between structural variations and antimicrobial activity. *J Biol Chem 281*, 19861-19871.

(23) Morgera, F., Vaccari, L., Antcheva, N., Scaini, D., Pacor, S., and Tossi, A. (2009) Primate cathelicidin orthologues display different structures and membrane interactions. *Biochem J 417*, 727-735.

(24) Zanetti, M., Gennaro, R., and Romeo, D. (1997) The cathelicidin family of antimicrobial peptide precursors: a component of the oxygen-independent defense mechanisms of neutrophils. *Ann N Y Acad Sci 832*, 147-162.

(25) Skerlavaj, B., Gennaro, R., Bagella, L., Merluzzi, L., Risso, A., and Zanetti, M. (1996) Biological characterization of two novel cathelicidin-derived peptides and identification of structural requirements for their antimicrobial and cell lytic activities. *J Biol Chem 271*, 28375-28381.

(26) Asthana, N., Yadav, S. P., and Ghosh, J. K. (2004) Dissection of antibacterial and toxic activity of melittin: a leucine zipper motif plays a crucial role in determining its hemolytic activity but not antibacterial activity. *J Biol Chem 279*, 55042-55050.

(27) Ahmad, A., Yadav, S. P., Asthana, N., Mitra, K., Srivastava, S. P., and Ghosh, J. K. (2006) Utilization of an amphipathic leucine zipper sequence to design antibacterial peptides with simultaneous modulation of toxic activity against human red blood cells. *J Biol Chem 281*, 22029-22038.

(28) Fields, G. B., and Noble, R. L. (1990) Solid phase peptide synthesis utilizing 9-fluorenylmethoxycarbonyl amino acids. *Int J Pept Protein Res 35*, 161-214.

(29) Yadav, S. P., Kundu, B., and Ghosh, J. K. (2003) Identification and characterization of an amphipathic leucine zipper-like motif in Escherichia coli

toxin hemolysin E. Plausible role in the assembly and membrane destabilization. *J Biol Chem 278*, 51023-51034.

(30) Oren, Z., and Shai, Y. (1997) Selective lysis of bacteria but not mammalian cells by diastereomers of melittin: structure-function study. *Biochemistry 36*, 1826-1835.

(31) Sal-Man, N., Oren, Z., and Shai, Y. (2002) Preassembly of membrane-active peptides is an important factor in their selectivity toward target cells. *Biochemistry 41*, 11921-11930.

(32) Mangoni, M. L., Maisetta, G., Di Luca, M., Gaddi, L. M., Esin, S., Florio, W., Brancatisano, F. L., Barra, D., Campa, M., and Batoni, G. (2008) Comparative analysis of the bactericidal activities of amphibian peptide analogues against multidrug-resistant nosocomial bacterial strains. *Antimicrob Agents Chemother 52*, 85-91.

(33) Nordahl, E. A., Rydengard, V., Morgelin, M., and Schmidtchen, A. (2005) Domain 5 of high molecular weight kininogen is antibacterial. *J Biol Chem 280*, 34832-34839.

(34) Papo, N., Braunstein, A., Eshhar, Z., and Shai, Y. (2004) Suppression of human prostate tumor growth in mice by a cytolytic D-, L-amino Acid Peptide: membrane lysis, increased necrosis, and inhibition of prostate-specific antigen secretion. *Cancer Res 64*, 5779-5786.

(35) Yadav, S. P., Ahmad, A., Pandey, B. K., Verma, R., and Ghosh, J. K. (2008) Inhibition of lytic activity of Escherichia coli toxin hemolysin E against human

red blood cells by a leucine zipper peptide and understanding the underlying mechanism. *Biochemistry 47*, 2134-2142.

(36) Sims, P. J., Waggoner, A. S., Wang, C. H., and Hoffman, J. F. (1974) Studies on the mechanism by which cyanine dyes measure membrane potential in red blood cells and phosphatidylcholine vesicles. *Biochemistry 13*, 3315-3330.

(37) Loew, L. M., Rosenberg, I., Bridge, M., and Gitler, C. (1983) Diffusion potential cascade. Convenient detection of transferable membrane pores. *Biochemistry 22*, 837-844.

(38) Zhang, L., Rozek, A., and Hancock, R. E. (2001) Interaction of cationic antimicrobial peptides with model membranes. *J Biol Chem 276*, 35714-35722.

(39) Pan, Y. L., Cheng, J. T., Hale, J., Pan, J., Hancock, R. E., and Straus, S. K. (2007) Characterization of the structure and membrane interaction of the antimicrobial peptides aurein 2.2 and 2.3 from Australian southern bell frogs. *Biophys J 92*, 2854-2864.

(40) Hawrani, A., Howe, R. A., Walsh, T. R., and Dempsey, C. E. (2008) Origin of low mammalian cell toxicity in a class of highly active antimicrobial amphipathic helical peptides. *J Biol Chem 283*, 18636-18645.

(41) Allen, T. M., and Cleland, L. G. (1980) Serum-induced leakage of liposome contents. *Biochim Biophys Acta 597*, 418-426.

(42) Greenfield, N., and Fasman, G. D. (1969) Computed circular dichroism spectra for the evaluation of protein conformation. *Biochemistry 8*, 4108-4116.

(43) Wu, C. S., Ikeda, K., and Yang, J. T. (1981) Ordered conformation of polypeptides and proteins in acidic dodecyl sulfate solution. *Biochemistry 20*, 566-570.

(44) Javadpour, M. M., and Barkley, M. D. (1997) Self-assembly of designed antimicrobial peptides in solution and micelles. *Biochemistry 36*, 9540-9549.

(45) Giddings, K. S., Johnson, A. E., and Tweten, R. K. (2003) Redefining cholesterol's role in the mechanism of the cholesterol-dependent cytolysins. *Proc Natl Acad Sci U S A 100*, 11315-11320.

(46) Sekar, R. B., and Periasamy, A. (2003) Fluorescence resonance energy transfer (FRET) microscopy imaging of live cell protein localizations. *J Cell Biol 160*, 629-633.

(47) Chigaev, A., Buranda, T., Dwyer, D. C., Prossnitz, E. R., and Sklar, L. A. (2003) FRET detection of cellular alpha4-integrin conformational activation. *Biophys J 85*, 3951-3962.

(48) Wouters, F. S., and Bastiaens, P. I. (2001) Imaging protein-protein interactions by fluorescence resonance energy transfer (FRET) microscopy. *Curr Protoc Protein Sci Chapter 19*, Unit19 5.

(49) Van Munster, E. B., Kremers, G. J., Adjobo-Hermans, M. J., and Gadella, T. W., Jr. (2005) Fluorescence resonance energy transfer (FRET) measurement by gradual acceptor photobleaching. *J Microsc 218*, 253-262.

(50) Dhe-Paganon, S., Werner, E. D., Nishi, M., Hansen, L., Chi, Y. I., and Shoelson, S. E. (2004) A phenylalanine zipper mediates APS dimerization. *Nat Struct Mol Biol 11*, 968-974.

(51) Ciornei, C. D., Sigurdardottir, T., Schmidtchen, A., and Bodelsson, M. (2005) Antimicrobial and chemoattractant activity, lipopolysaccharide neutralization, cytotoxicity, and inhibition by serum of analogs of human cathelicidin LL-37. *Antimicrob Agents Chemother 49*, 2845-2850.

(52) Oren, Z., Lerman, J. C., Gudmundsson, G. H., Agerberth, B., and Shai, Y. (1999) Structure and organization of the human antimicrobial peptide LL-37 in phospholipid membranes: relevance to the molecular basis for its non-cell-selective activity. *Biochem J 341 (Pt 3)*, 501-513.

(53) Porcelli, F., Buck-Koehntop, B. A., Thennarasu, S., Ramamoorthy, A., and Veglia, G. (2006) Structures of the dimeric and monomeric variants of magainin antimicrobial peptides (MSI-78 and MSI-594) in micelles and bilayers, determined by NMR spectroscopy. *Biochemistry 45*, 5793-5799.

Table-1: Amino acid sequences of BMAP-27 and its analogs

Peptides	**Amino acid sequences** (X=H, NBD or Rhodamine) (Amino acids at 'a' and 'd' positions are bold and substituted amino acids are boldface and underlined)
	f g a b c d e f g a b c d e f g a b c d e f g a b c
BMAP-27	X-NH- G R **F** K R **F** R K K **F** K K **L** F K K **L** S P **V** I P L **L** H L $CONH_2$
Mu-1 BMAP-27	X-NH- G R F K R F R K K **A** K K L F K K L S P **V** I P L **L** H L -$CONH_2$
Mu-2 BMAP-27	X-NH- G R F K R F R K K F K K L F K K **A** S P **V** I P L **L** H L -$CONH_2$
Mu-3 BMAP-27	X-NH- G R **A** K R F R K K **A** K K L F K K L S P **V** I P L **L** H L -$CONH_2$
Mu-4 BMAP-27	X-NH- G R F K R F R K K F K K **A** F K K **A** S P **V** I P L **L** H L -$CONH_2$

Table-2: Antibacterial activity of BMAP-27 and its analogs

Minimal inhibitory concentration (MIC) in μM				
Peptides / antibiotic	***S. aureus* ATCC 9144**	***B. subtilis* ATCC 6633**	***E.coli* DH5α**	***E. Coli* ATCC 10536**
BMAP-27	2.7 ±0.8	2.6 ±0.7	2.8 ± 0.6	3.2 ±0.9
Mu-1 BMAP-27	2.8 ± 0.8	2.7 ± 0.7	2.9 ± 0.6	3.2 ± 0.9
Mu-2 BMAP-27	2.8 ± 0.8	2.7 ± 0.7	2.9 ± 0.6	2.9 ± 0.9
Mu-3 BMAP-27	2.7 ± 0.8	2.8 ± 0.7	2.9 ± 0.8	2.9 ± 0.9
Mu-4 BMAP-27	2.7 ± 0.8	2.9 ± 0.7	2.9 ± 0.6	2.7 ± 0.9
Tetracycline	1.0 ± 0.2	1.0 ± 0.2	1.2 ± 0.2	1.2 ± 0.9

MIC values are the mean of three independent experiments each performed in duplicate ±SD.

Figure Legends:

Figure-1: The decrease in toxic activity of the BMAP-27 against hRBC and murine 3T3 cells after substitution of leucine/phenylalanine residues at 'a' and/or 'd' position by alanine. (**A**), Dose-dependent hemolytic activity assay of the BMAP-27, solid square; Mu-1 BMAP-27, solid circle; Mu-2 BMAP-27, open circle; Mu-3 BMAP-27, solid triangle; and Mu-4 BMAP-27, open triangle. (**B**), Dose-dependent MTT assay of 3T3 cells in the presence of BMAP-27, solid square; Mu-1 BMAP-27, solid circle; Mu-2 BMAP-27, open circle; Mu-3 BMAP-27, solid triangle; and Mu-4 BMAP-27, open triangle. Each point represents the mean result of three independent experiments and error bar indicates SD.

Figure-2: Determination of peptide-induced membrane damage of Murine 3T3 cells by flow cytometric studies. Panels A to F show the PI staining of Murine 3T3 cells without any peptide treatment and treated with ~10.0 μM of BMAP-27, Mu-1 BMAP-27, Mu-2 BMAP-27, Mu-3 BMAP-27 and Mu-4 BMAP-27 respectively. On Y axis, FSC-Height is forward scattered height which shows the distribution of the cells. In X axis, FL2-Height means fluorescence recorded by fluorescent filter 2 (red channel). 10,000 events were counted for each experiment.

Figure 3: Determination of peptide-induced membrane damage of *E. coli* cells by flow cytometric studies. Panels A to F show the PI staining of *E. coli* cells without any peptide treatment and treated with ~3.5 μM of BMAP-27, Mu-1 BMAP-27, Mu-2 BMAP-27, Mu-3 BMAP-27 and Mu-4 BMAP-27 respectively. On Y axis, FSC-Height (H) means forward scattered height which shows the distribution of the cells. In X axis,

FL2-Height means fluorescence recorded by fluorescent filter 2 (red channel). 10,000 events were counted for each experiment.

Figure-4: Dose-dependent peptide-induced transmembrane depolarization of *E. coli* and hRBC. (A) and (B) show the plot of the percentage of fluorescence recovery, which is a measure of transmembrane depolarization, vs. peptide concentration in μM of *E. coli* and hRBCs respectively. Symbols: solid square, BMAP-27; solid circle, Mu-1 BMAP-27, open circle, Mu-2 BMAP-27, solid triangle, Mu-3 BMAP-27 and open triangle, Mu-4 BMAP-27. Each point represents the mean result of three independent experiments and error bar indicates SD.

Figure-5: Permeabilization of zwitterionic and negatively charged lipid vesicles by BMAP-27 and its analogs as studied by the dissipation of diffusion potentials induced by the individual peptides. Panel A: shows the profiles of dissipation of diffusion potential of zwitterionic PC/Chol lipid vesicles in the presence of BMAP-27 and its analogs with peptide concentration for each of the peptides at ~6.1 μM**.** Panel B shows the profiles of dissipation of diffusion potential of negatively charged PC/PG lipid vesicles induced by BMAP-27 and its analogs with peptide concentration for each of the peptides at ~4.6 μM**.** Symbols for panels A and B are: BMAP-27, solid; Mu-1 BMAP-27, dash; Mu2 BMAP-27, dot; Mu-3 BMAP-27, dash dot and Mu-4 BMAP-27, dash dot dot line respectively. Panels C and D show the column plots of fluorescence recovery induced by BMAP-27 and its analogs in PC/Chol and PC/PG lipid vesicles respectively. All the peptides were employed at equal but five different concentrations as marked in the X-axis of the plots. The columns a, b, c, d and e represent BMAP-27, Mu-1 BMAP-27, Mu-2 BMAP-27, Mu-3 BMAP-27 and Mu-4 BMAP-27 respectively. Concentration of PC/Chol and

PC/PG lipid vesicles was 68 μM. Each point represents the mean result of three independent experiments and error bar indicates SD.

Figure-6: Determination of secondary structures of 21.0 μM of BMAP-27 and its analogs in the presence of 40% TFE (in water, v/v) (A) and 1% SDS (B). Symbols are: BMAP-27, solid; Mu-1 BMAP-27, dash; Mu2 BMAP-27, dot; Mu-3 BMAP-27, dash dot and Mu-4 BMAP-27, dash dot dot.

Figure-7: Detection of localization of the Rho-labeled BMAP-27, Rho-labeled Mu-1 BMAP-27 and Rho-labeled Mu-4 BMAP-27 onto hRBCs and *E.coli* DH5α by confocal microscopy. Each cell type has been marked on top of the figure and Rho-labeled peptides, BMAP-27; Mu-1 BMAP-27 (in short Mu-1) and Rho-labeled Mu-4 BMAP-27 (in short Mu-4) that have been used to treat the cells are shown on the left hand side. For each of peptide treatment fluorescence and DIC images of each cell type have been shown. Peptide concentration of each of the Rho-labeled peptides for treatment with hRBCs was ~12 μM whereas for treatment with *E. coli* at < MIC was ~ 2.0 μM and at MIC was ~ 3.0 μM. hRBCs were plated on poly-L-lysine coated slide and incubated with Rhodamine labeled peptides for 15 min in PBS. Afterward cells were fixed in 2% paraformaldehyde (10 min.) and washed extensively with PBS. Before confocal scanning (Oil immersion, 63x, crop size: 2) slides were mounted with 80% glycerol containing antifade.

Similarly, log phase *E. coli* were incubated with Rhodamine labeled peptides for 15 min at different concentration (MIC and 70% of MIC) and placed on Poly-L-lysine coated slides. Afterward cells were fixed with 2% paraformaldehyd (10 min.) and washed

extensively. Before confocal scanning (oil immersion,63X, crop size:2) sample were mounted with 80% glycerol containing antifade.

Figure 8: Detection of self-assembly of the BMAP-27, Mu-1 BMAP-27 and Mu-4 BMAP-27. onto the *E. coli and* hRBCs cells by FRET experiments with the help of flow cytometry. Equimolar amounts of donor- (NBD) labeled peptides (D) and either the corresponding unlabeled peptide (U) or acceptor- (Rho) labeled peptide (A) incubated with hRBCs [(A) to (C)] and *E. coli* cells (D) to (F) at 37^0C and then analyzed by flow cytometry. Black (thinner) and gray (thicker) lines represent (D+U) and (D+A) respectively. (A) to (C) show the FRET experiments onto hRBCs with BMAP-27, Mu-1 BMAP-27 and Mu-4 BMAP-27 respectively with ~12.0 μM of each of the peptides. While (D) to (F) show the FRET experiments onto *E. coli* cells with the same peptides at ~ 3.0 μM concentration. The numerical values shown on the profiles represent the mean fluorescence intensities. 10,000 events were counted for each of these experiments. Panels G and H show the percentage of energy transfer (described in the Materials and Methods) observed with different peptides as marked in the figure onto hRBCs and *E. coli* respectively. Each % of FRET value represents the mean result of two independent experiments and error bar indicates SD.

Biochemistry, 2009, 48(46), 10905-17

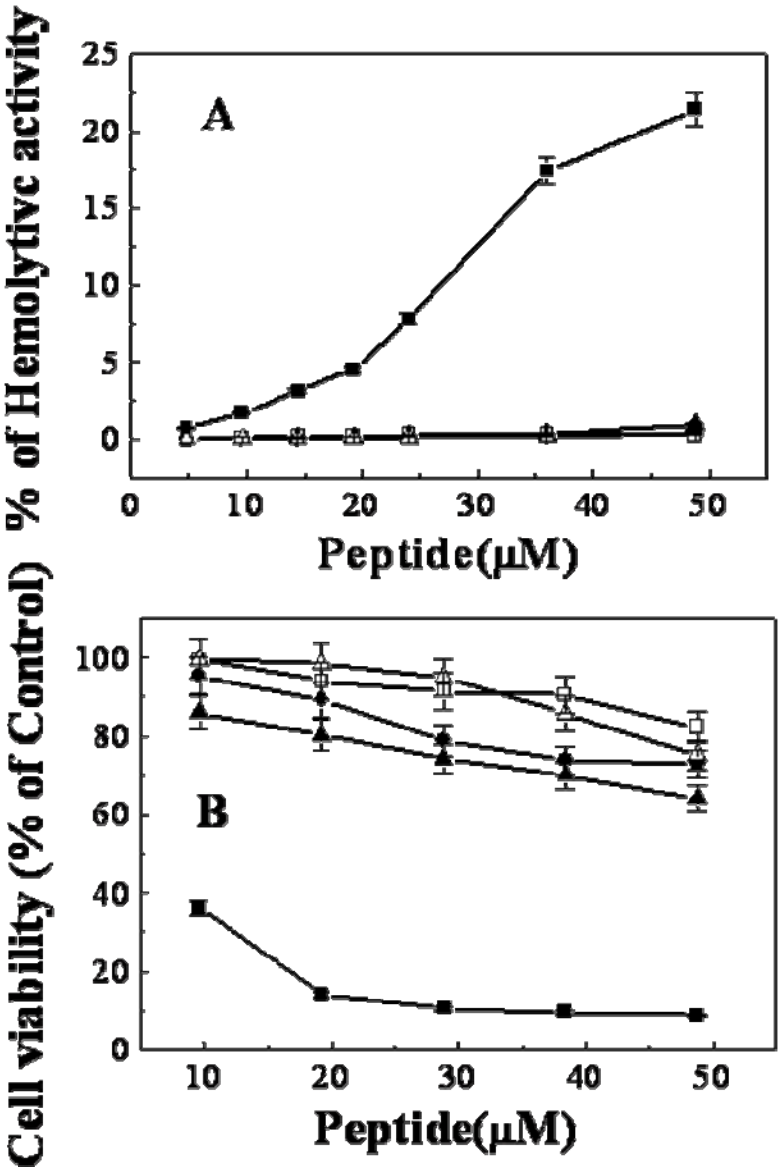

Figure-1

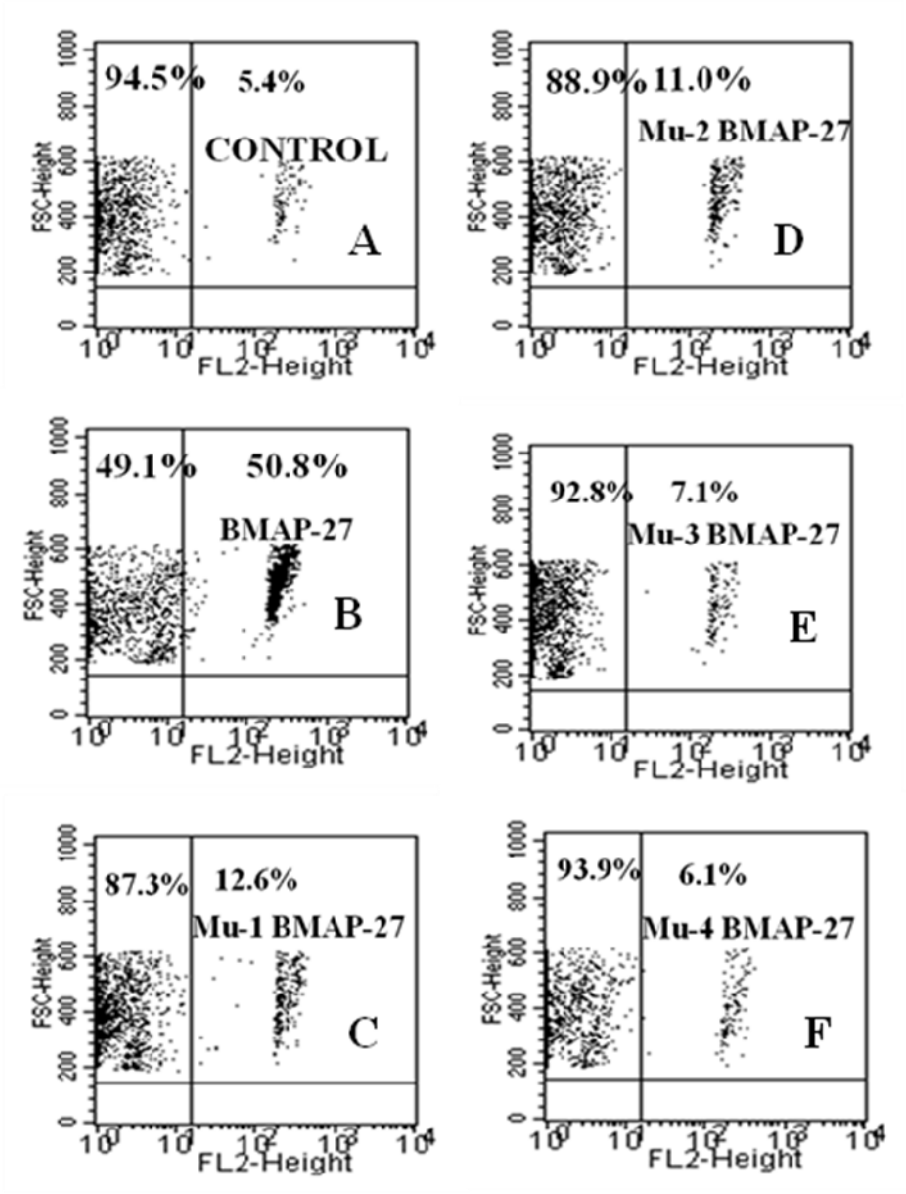
94.5%
5.4%
CONTROL
A
88.9%
11.0%
Mu-2 BMAP-27
D
49.1%
50.8%
BMAP-27
B
92.8%
7.1%
Mu-3 BMAP-27
E
87.3%
12.6%
Mu-1 BMAP-27
C
93.9%
6.1%
Mu-4 BMAP-27
F
FSC-Height
FL2-Height

Figure-2

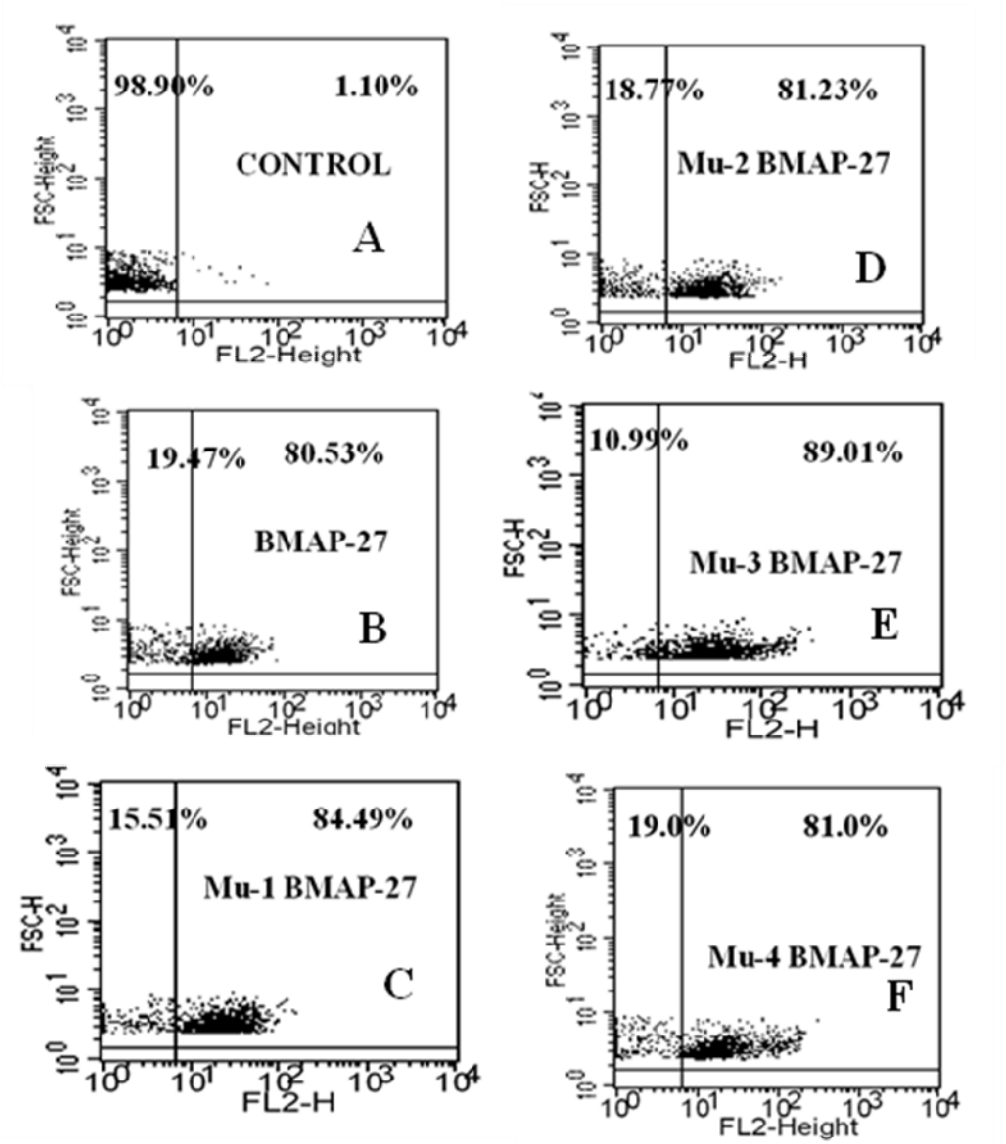
98.90%
1.10%
CONTROL
A
FSC-Height
FL2-Height
18.77%
81.23%
Mu-2 BMAP-27
D
FSC-H
FL2-H
19.47%
80.53%
BMAP-27
B
FSC-Height
FL2-Height
10.99%
89.01%
Mu-3 BMAP-27
E
FSC-H
FL2-H
15.51%
84.49%
Mu-1 BMAP-27
C
FSC-H
FL2-H
19.0%
81.0%
Mu-4 BMAP-27
F
FSC-Height
FL2-Height

Figure-3

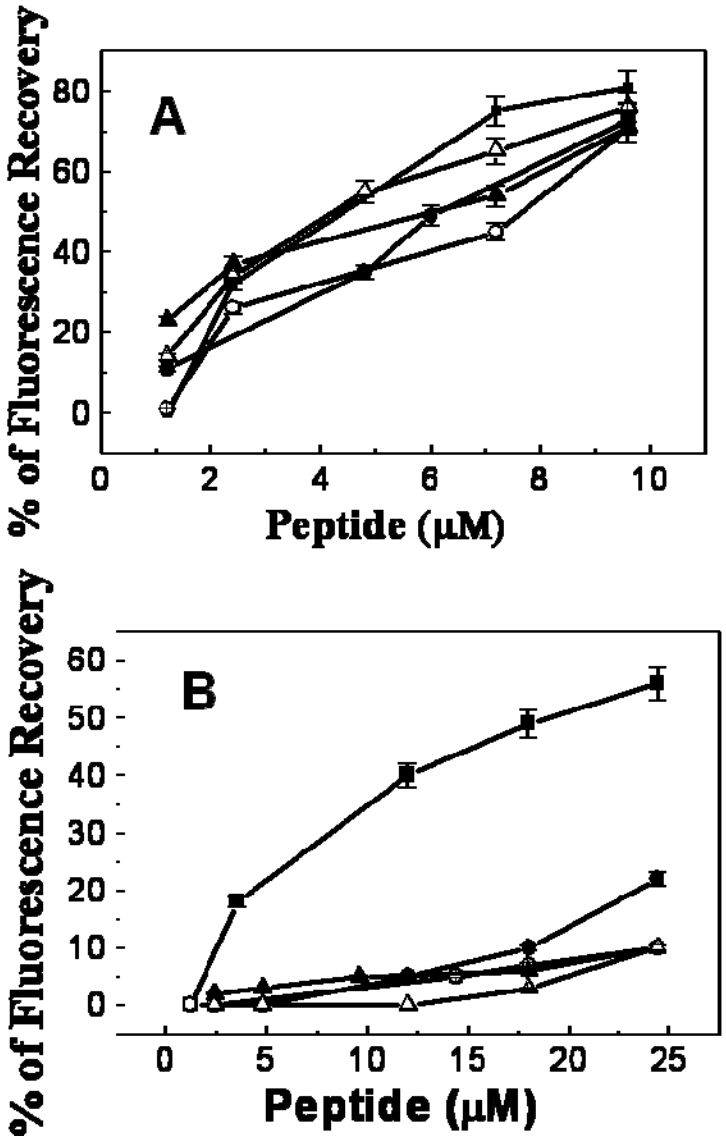
A
% of Fluorescence Recovery
0
20
40
60
80
0
2
4
6
8
10
Peptide (μM)
B
% of Fluorescence Recovery
0
10
20
30
40
50
60
0
5
10
15
20
25
Peptide (μM)

Figure-4

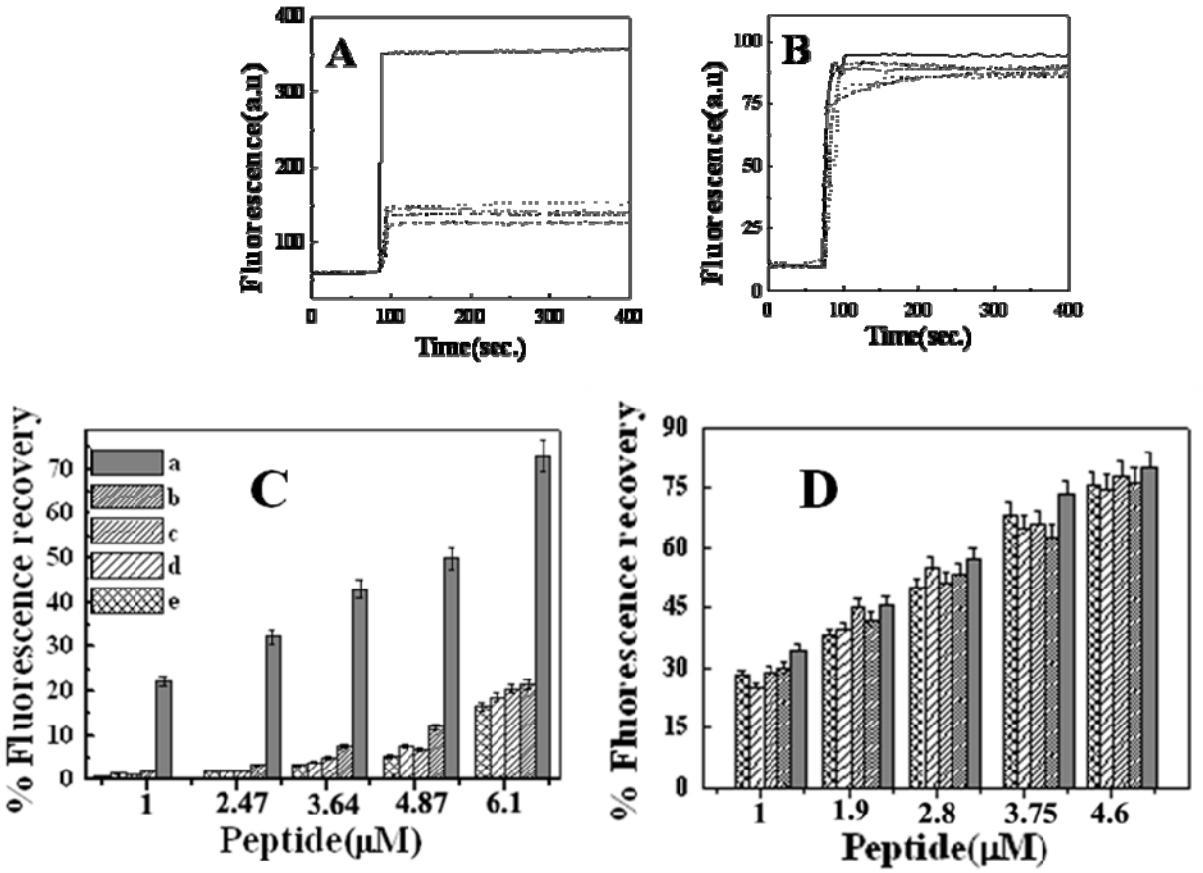
A
Fluorescence(a.u)
Time(sec.)
B
Fluorescence(a.u)
Time(sec.)
C
% Fluorescence recovery
a
b
c
d
e
1
2.47
3.64
4.87
6.1
Peptide(μM)
D
% Fluorescence recovery
1
1.9
2.8
3.75
4.6
Peptide(μM)

Figure-5

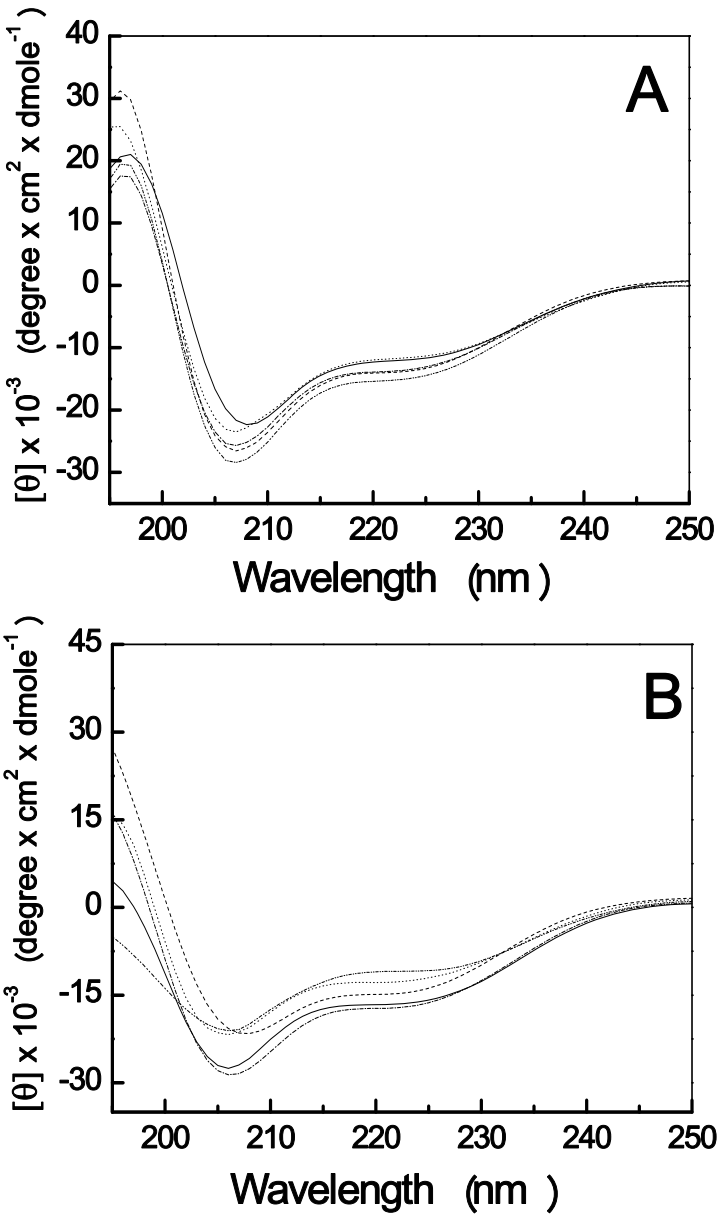
A
[θ] x 10^-3 (degree x cm^2 x dmole^-1)
40
30
20
10
0
-10
-20
-30
200
210
220
230
240
250
Wavelength (nm)
B
[θ] x 10^-3 (degree x cm^2 x dmole^-1)
45
30
15
0
-15
-30
200
210
220
230
240
250
Wavelength (nm)

Figure-6

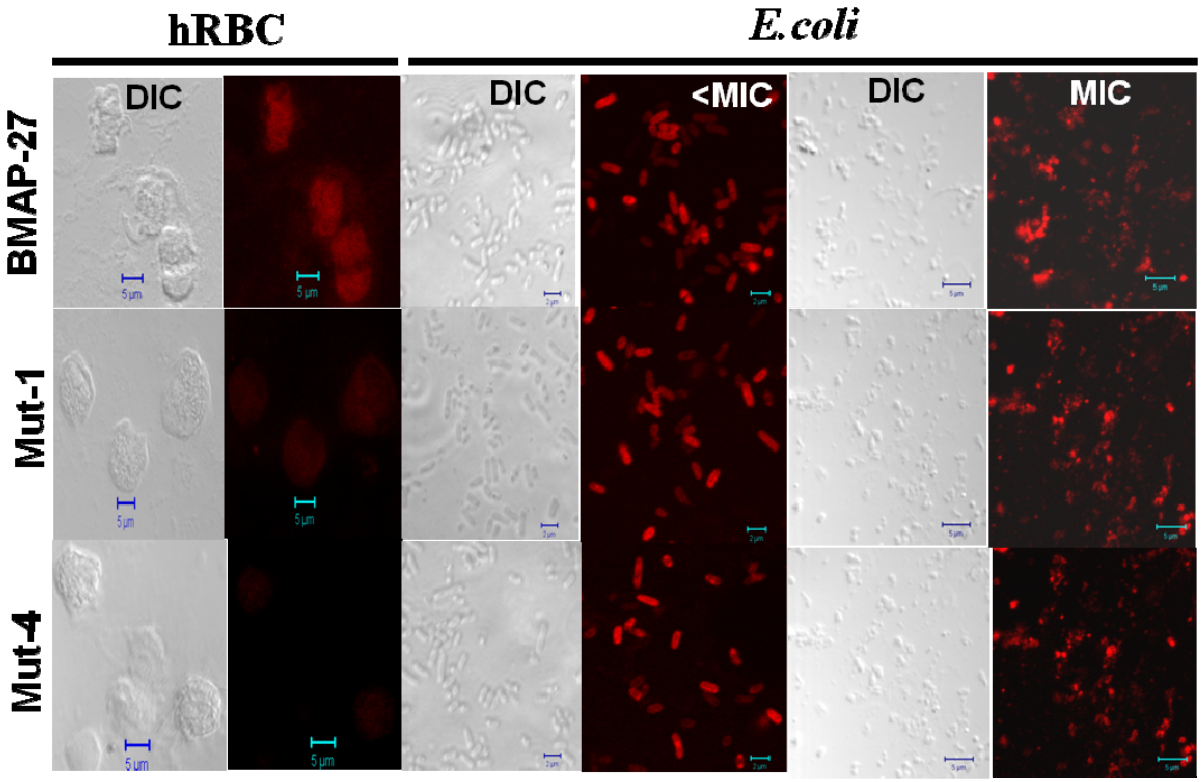

Figure-7

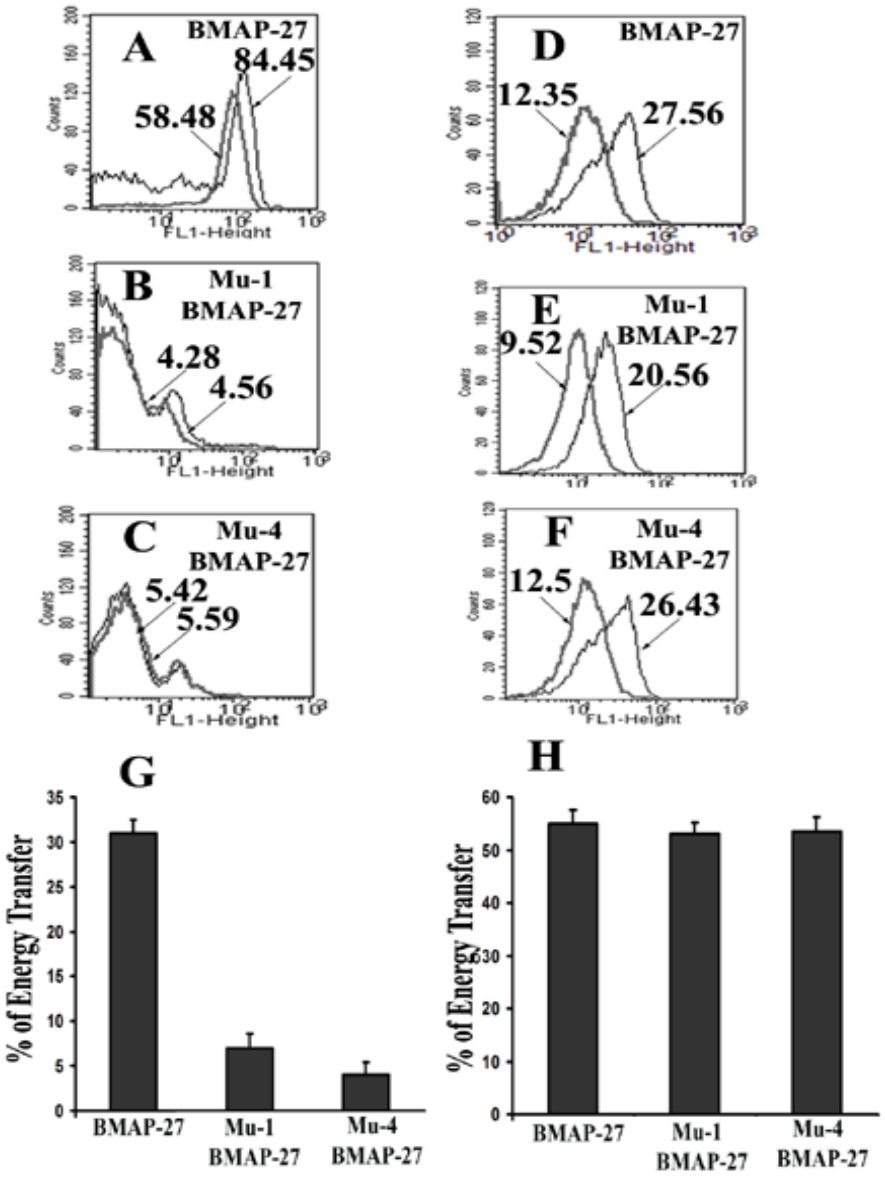
A
BMAP-27
84.45
58.48
B
Mu-1
BMAP-27
4.28
4.56
C
Mu-4
BMAP-27
5.42
5.59
D
BMAP-27
12.35
27.56
E
Mu-1
BMAP-27
9.52
20.56
F
Mu-4
BMAP-27
12.5
26.43
Counts
FL1-Height
G
% of Energy Transfer
BMAP-27
Mu-1
BMAP-27
Mu-4
BMAP-27
H
% of Energy Transfer
BMAP-27
Mu-1
BMAP-27
Mu-4
BMAP-27

Figure-8

Biochemistry, 2009, 48(46), 10905-17

FOR TABLE OF CONTENTS USE ONLY

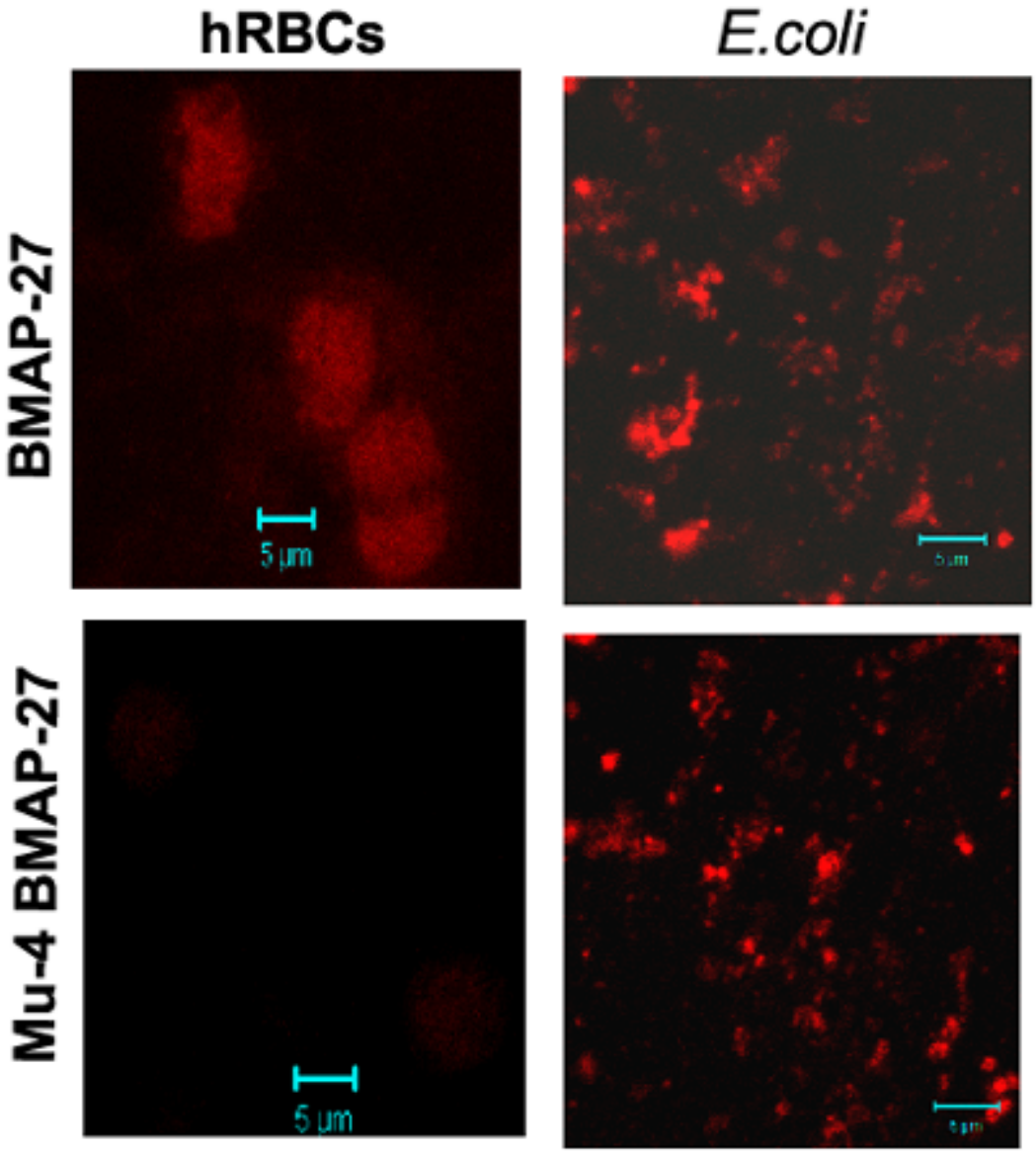

Title: Design of non-toxic analogs of cathelicidin-derived bovine anti-microbial peptide BMAP–27: The role of leucine as well as phenylalanine zipper sequences in determining its toxicity.

Biochemistry, 2009, 48(46), 10905-17

Authors: Aqeel Ahmad[1] Sarfuddin Azmi[1$], Raghvendra M. Srivastava[1$], Saurabh Srivastava[1], Brijesh K. Pandey[1], Rubha Saxena[1], Virendra Kumar Bajpai[2] and Jimut Kanti Ghosh[1]

Biochemistry, 2009, 48(46), 10905-17

SUPPORTING INFORMATION

Biochemistry, 2009, 48(46), 10905-17

Supplementary Table-1

Peptide	Minimal inhibitory concentration (MIC) in μM in presence of serum	
	E. coli **ATCC10536**	***B. subtilis*** **ATCC6633**
BMAP-27	**7.4±0.7**	**15.1±0.5**
Mu-1 BMAP-27	**7.4±0.7**	**14.8±0.6**
Mu-2 BMAP-27	**7.3±0.6**	**14.7±0.6**
Mu-3 BMAP-27	**7.3±0.6**	**15.0±0.8**
Mu-4 BMAP-27	**7.2±0.6**	**15.1±0.6**

MIC values are the mean of three independent experiments each performed in duplicate ±SD.

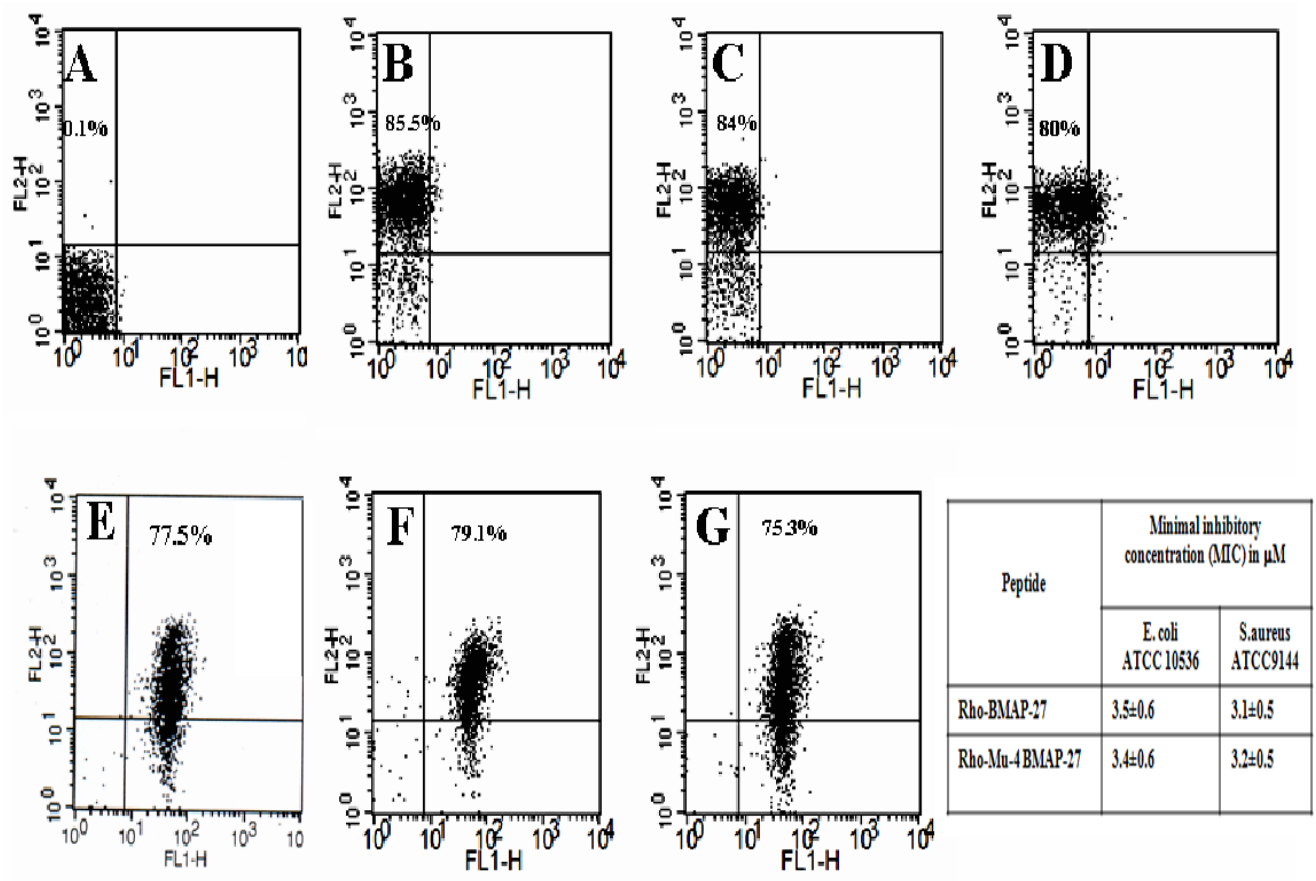

Peptide	Minimal inhibitory concentration (MIC) in μM	
	E. coli ATCC 10536	S.aureus ATCC9144
Rho-BMAP-27	3.5±0.6	3.1±0.5
Rho-Mu-4 BMAP-27	3.4±0.6	3.2±0.5

Supplementary Figure-1

PI staining of *E. coli.* ATCC 10536 after their incubation with BMAP-27, Mu-1 BMAP-27 and Mu-4 BMAP-27 (Panel B-D) and the corresponding NBD-labelled versions (Panel E-F). Panel A shows the control experiment of staining of bacteria without any peptide treatment. Concentration of the peptides was 4.2 μM. 10000 events were counted in each experiment. Panel H shows the antibacterial activity of Rho-labeled peptides. MIC values are the mean of three independent experiments each performed in duplicate ±SD.

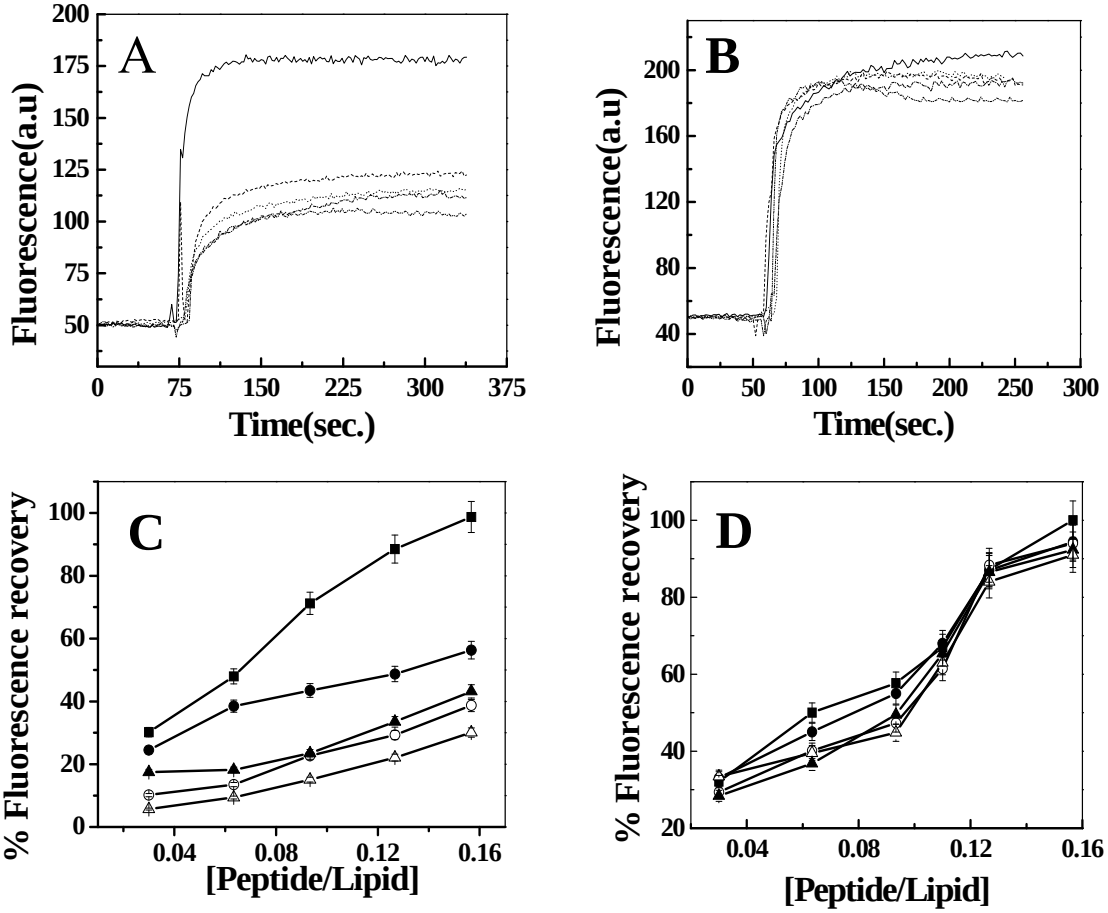

Supplementary Figure-2

Peptide-induced release of calcein from calcein-entrapped zwitterionic and negatively charged lipid vesicles in the presence of BMAP-27 and its analogs. Panel A: shows the profiles of fluorescence enhancement as a result of calcein release from zwitterionic PC/Chol lipid vesicles in the presence of BMAP-27 and its analogs with peptide concentration for each of the peptides at ~0.47 μM**.** Panel B shows the fluorescence profiles of calcein release from negatively charged PC/PG lipid vesicles induced by BMAP-27 and its analogs with peptide concentration for each of the peptides at ~0.47 μM**.** Symbols for panels A and B are: BMAP-27, solid; Mu-1 BMAP-27, dash; Mu2 BMAP-27, dot; Mu-3 BMAP-27, dash dot and Mu-4 BMAP-27, dash dot dot line respectively. Panels C and D show the plots of peptide/lipid molar ratios vs. fluorescence recovery induced by BMAP-27 and its analogs in PC/Chol and PC/PG lipid vesicles respectively. Symbols: solid square, BMAP-27; solid circle, Mu-1 BMAP-27, open circle, Mu-2 BMAP-27, solid triangle, Mu-3 BMAP-27 and open triangle, Mu-4 BMAP-27. Each point represents the mean result of three independent experiments and error bar indicates SD.

Biochemistry, 2009, 48(46), 10905-17

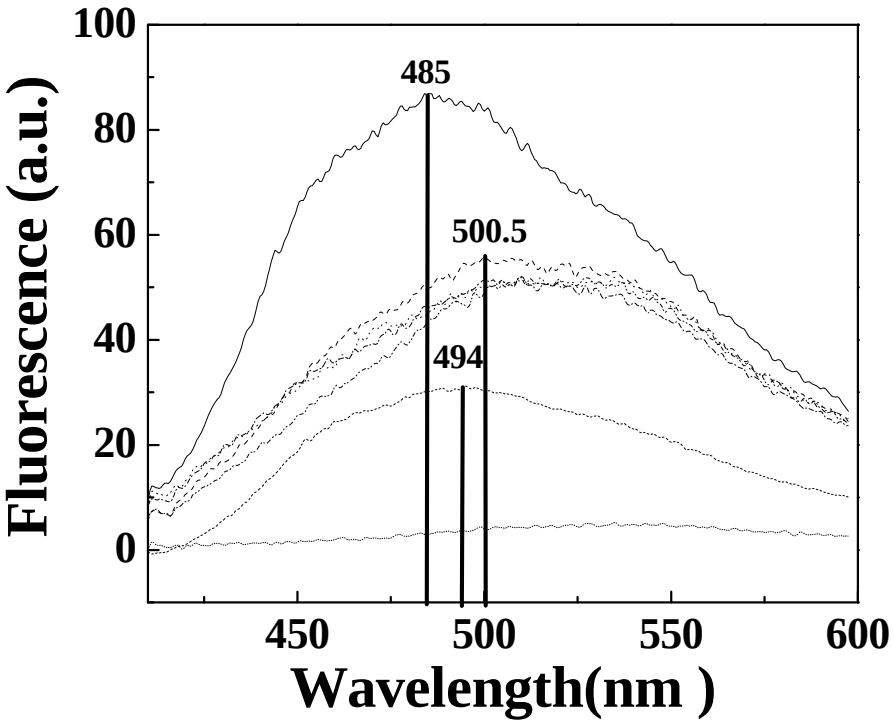

Supplementary Figure-3

ANS binding experiment of the BMAP-27, Mu-1 BMAP-27, Mu-2 BMAP-27, Mu-3 BMAP-27, Mu-4 BMAP-27 and SCR-BMAP-27 in PBS. BMAP-27, solid; Mu-1 BMAP-27, dash; Mu2 BMAP-27, dot; Mu-3 BMAP-27, dash dot, Mu-4 BMAP-27, dash dot dot and SCR-BMAP-27, short dash line respectively. Profile of only ANS in PBS shown by short dot. Numerical values at the top of some profile indicate wavelength of emission maxima. ANS concentration was ~ 20 μM and concentration of each of the peptides was ~ 47.0μM. The excitation wavelength was 365 nm and the excitation and emission slits were fixed at 6 and 4 nm respectively.

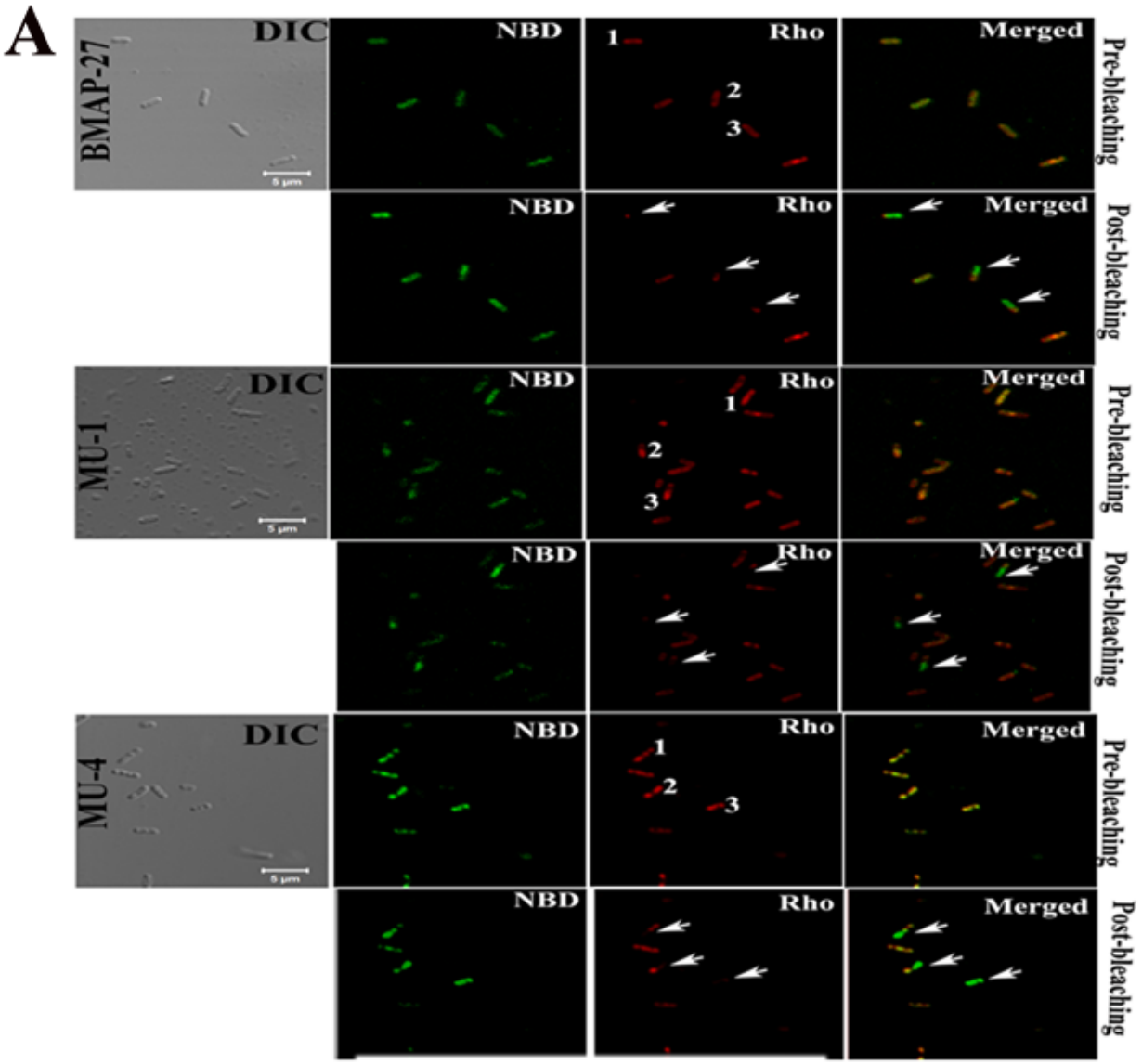
A
BMAP-27
DIC
NBD
Rho
Merged
Pre-bleaching
Post-bleaching
MU-1
MU-4
1
2
3
B
% FRET EFFICIENCY
40
30
20
10
0
BMAP-27
Mu-1 BMAP-27
Mu-4 BMAP-27

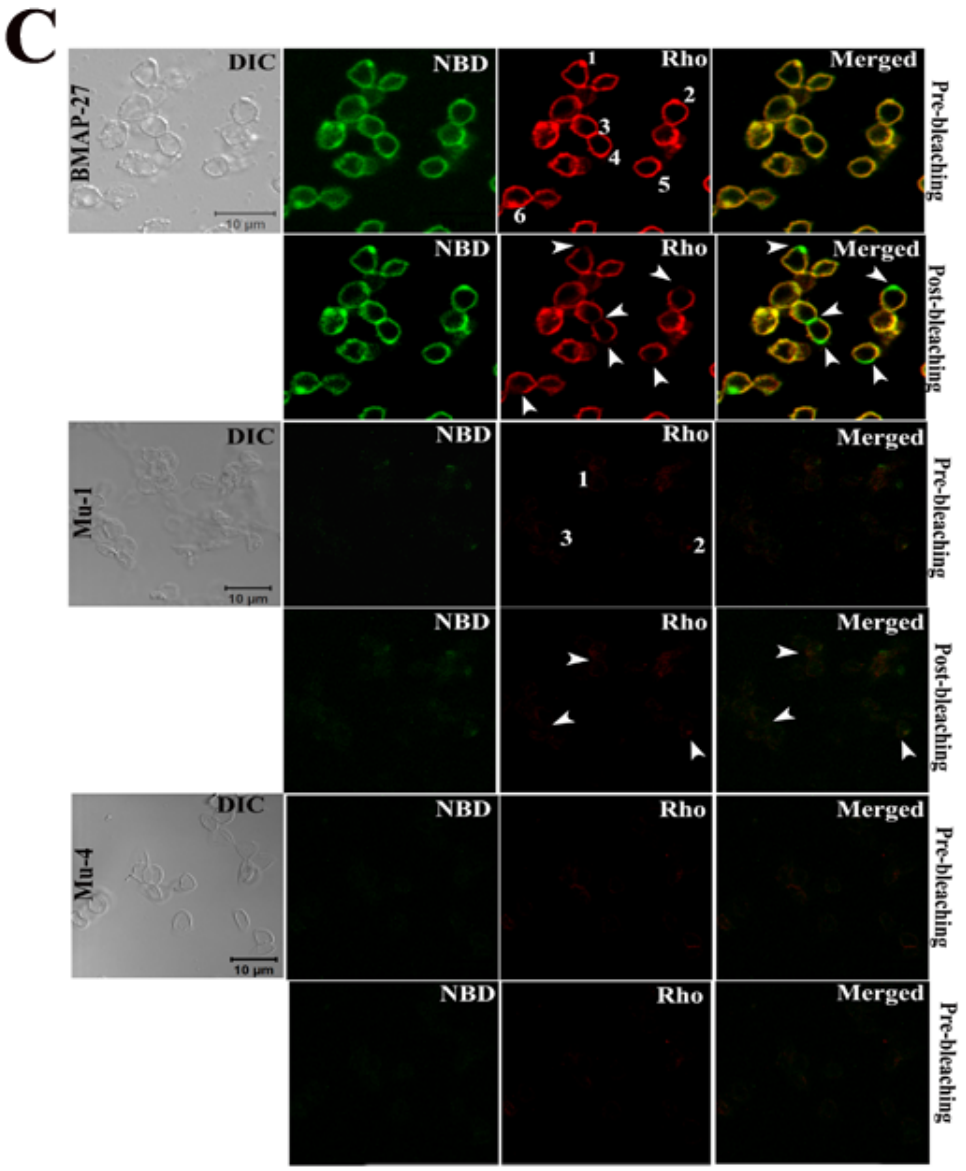
C
DIC
NBD
Rho
Merged
BMAP-27
Pre-bleaching
Post-bleaching
Mu-1
Mu-4
10 μm
1
2
3
4
5
6

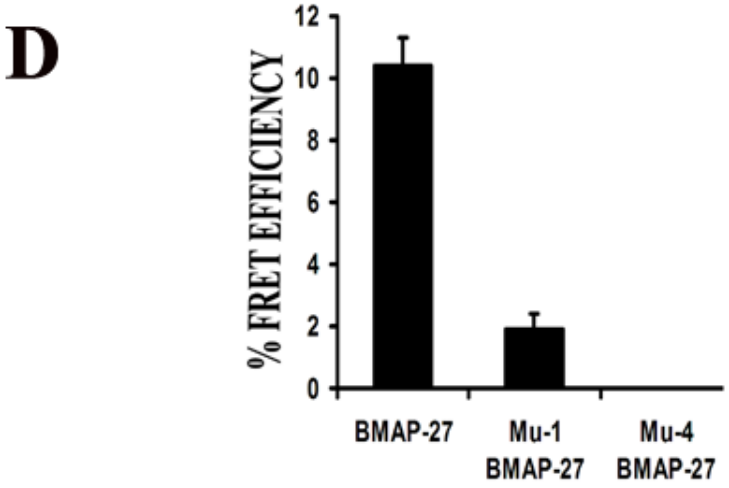
D
% FRET EFFICIENCY
12
10
8
6
4
2
0
BMAP-27
Mu-1 BMAP-27
Mu-4 BMAP-27

Biochemistry, 2009, 48(46), 10905-17

SUPPLEMENTRY FIGURE-4:

Fluorescence resonance energy transfer (FRET) experiments by confocal microscopic studies demonstrating the differential behaviour of BMAP-27 and its analogs towards *E. coli* (Figure 4A and B) and hRBCs (Figure 4C and D). DIC (bright field) images of bacteria and hRBCs are shown in left panels, NBD and Rho stands for the fluorescence of *E. coli* or hRBCs when they were bound to NBD and rhodamine labelled peptides respectively and merged implies for the collective fluorescence of the cells in the presence of Rho and NBD labelled peptides.

Figure 4A depicts the self-assembly of BMAP-27 and its selected analogs (Mu-1 BMAP-27 and Mu-4 BMAP-27; peptide concentration, 1.5 μM) on the bacterial membrane. In BMAP-27 upper panel (pre-bleach) images show the binding of NBD and Rho labelled BMAP-27 peptides onto *E. coli*. In merged images the co-localization of NBD and rhodamine labelled BMAP-27 peptides are shown. Numbers (1,2,3) in Rho images are the region of interests (ROI) that were selected for photobleaching. In post-bleach panel bleached Rho are shown with arrows; similarly enhanced NBD fluorescence are also shown in merged field with arrows. The FRET efficiency was calculated by comparing the fluorescence intensities of NBD that indirectly demonstrate FRET (quantam of energy transfer before photobleaching). Similar to the BMAP-27, FRET analysis were performed in Mu-1-BMAP-27 and Mu-4-BMAP-27, numbers (1,2,3) demonstrate the region of interest in pre-bleached state, and arrows in Rho images indicate the bleached acceptor and enhanced NBD fluorescence in the merged images. All the images were captured on scan zoom5 and multiple random regions of interests in each field were selected to evaluate FRET. Data is the representative of 2 different experiments for each sample. The average of the fluorescence intensity values (%FRET efficiency) calculated (described in Materials and Methods) for BMAP-27, Mu-1 BMAP-27 and Mu-4 BMAP-27 peptides from each region of interests shown in Figure 4B**,** which exhibits the comparable self aggregation behaviour of BMAP-27 and its analogs.

Figure 4C shows *the* energy transfer of BMAP-27 and its analogs (peptide concentration, 6.0 μM) onto hRBCs. The pattern of pre- and post-bleach panels are the same as that described in figure 4A. BMAP-27 peptide shows a considerable co-localization on RBCs membrane whereas the Mu-1-BMAP-27 and Mu-4-BMAP-27 failed to do the same. The numbers of ROIs selected in BMAP-27 are more than Mu-1- BMAP-27 to represent the energy transfer more significantly.

To make the images more comprehensible in terms energy transfer we have also chosen the larger zoom size (4) for BMAP-27 than analogs (scan zoom size 3). The extent of energy transfer was calculated by similar method as in bacteria. The Figure 4D shows the average numerical values of percentage energy transfer for different peptides onto hRBCs..

Peptide	Amino acids sequence (Amino acids with interchanged positions are marked by underline)
SCR- BMAP-27	H_2N-F R F K R F R K K G K K L F K K V S P P I L L L H L-$CONH_2$

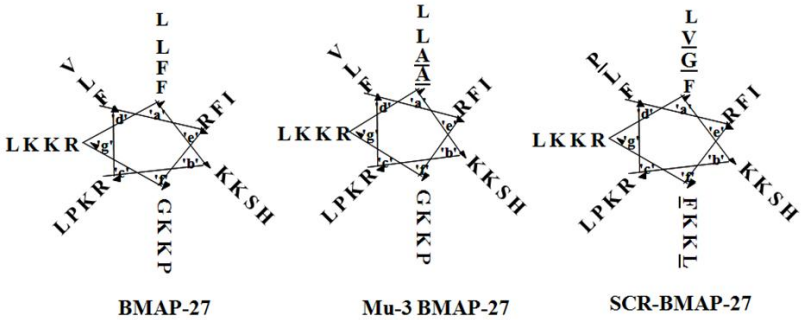

Peptide	Minimal inhibitory concentration (MIC) in μM			
	E.coli(DH5α)	*E. coli* ATCC10536	*S. aureus* ATCC9144	*B. subtilis* ATCC 6633
SCR-BMAP-27	3.1±0.6	3.3±0.7 (8.1±0.7)	3.2±0.6	3.0±0.6 (15.3±0.7)

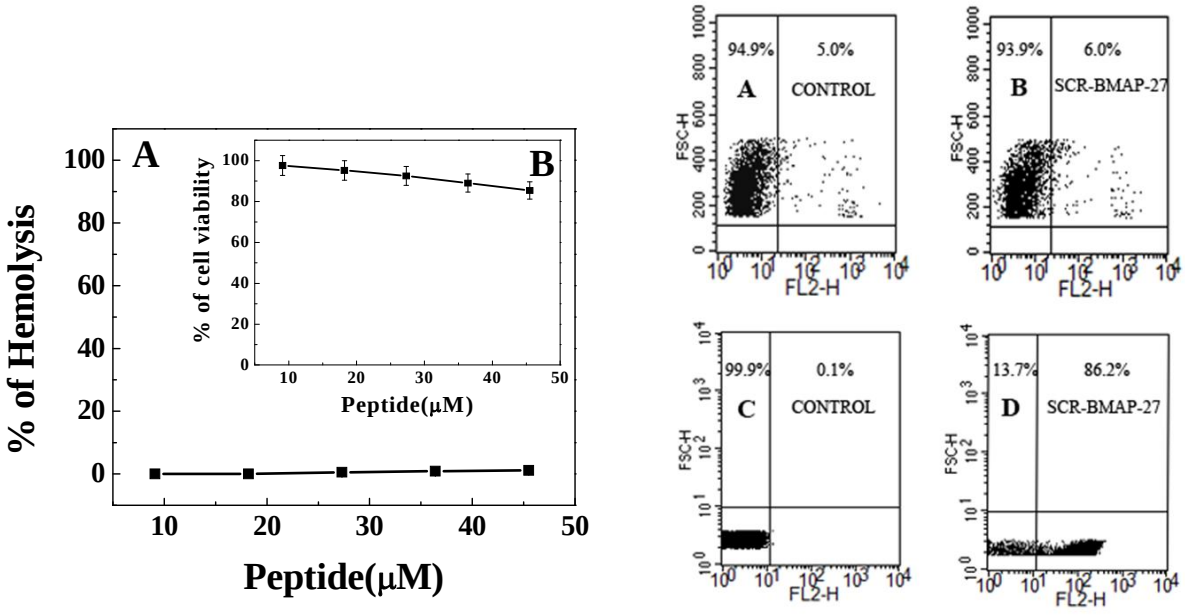

Supplementary Figure-5

Legends of supplementary figure-5

(1) Amino acid sequence of SCR-BMAP-27

(2) Helical wheel projections of BMAP-27, Mu-3 BMAP-27 and SCR-BMAP-27. Mutated positions are shown as underlined.

(3) Antimicrobial activity of SCR-BMAP-27 against different microorganisms and values in parentheses shows MIC in presence of serum for *E. coli* ATCC 10536 and *B. subtilis* ATCC 6633. MIC values are the mean of three independent experiments each performed in duplicate ±SD.

(4) Panel A shows the plot of hemolytic activity assay of SCR-BMAP-27against hRBCs

Inset (Panel B) shows the plot of cell viability assay of SCR-BMAP-27 against murine 3T3 cell lines

(5) Panels A and B show PI staining of murine 3T3 cells in the absence and presence of peptide respectively (Peptide concentration: 10 μM)

Panels C and D show PI staining of *E. coli*. DH5α in the absence and presence of peptide respectively (peptide concentration: 3.5 μM)